PlaneRay: An acoustic underwater propagation model based on ray tracing and plane-wave reflection coefficients

Jens M. Hovem

Forsvarets forskningsinstitutt/Norwegian Defence Research Establishment (FFI)

10.03.2008

FFI-rapport 2008/00610

1027

P: ISBN 798-82-464-1437-9
E: ISBN 798-82-464-1438-6

Keywords

Undervannsakustikk / Underwater acoustics

Akustisk bølgeutbredelse / Acoustic wave propagation

Strålegangs beregninger / Ray tracing

Approved by

Torgeir Svolsbru	Project Manager
Elling Tveit	Director of Research
John-Mikal Størdal	Director

English summary

PlaneRay is a ray tracing program for underwater acoustic propagation modeling that can treat moderately range-varying scenarios. The model uses a unique sorting and interpolation routine for efficient determination of a large number of eigenrays connecting a source with a large number of receivers positioned on a horizontal line. No rays are traced into the bottom, but the bottom interaction is modeled by local plane wave reflection coefficients. The bottom can be a fluid sedimentary layer over an elastic half space and the layer thickness and the sound speeds and the densities of the sediment and the elastic medium can vary with range. The sound speed of the water may vary with depth, but not with range. For each eigenray the model calculates the trajectories, travel times and amplitudes and constructs the complete frequency response by coherent addition of all the multiple arrivals. By multiplying the frequency spectrum with the spectrum of a source signal and inverse Fourier transforming the product, the complete time response at any position on the receiving line is synthesized. The paper gives a description of the model and presents a number of illustrative cases. Important considerations are the accuracy of the ray model and how accurate the plane wave reflection coefficients can represent the effects of a layered bottom. This problem is discussed by comparing the time and frequency domains solution of the ray model with the results from established models based on the wave number integration and the parabolic equation.

Sammendrag

PlaneRay er modell for beregning av akustisk bølgeutbredelse i sjøen som kan anvendes i situasjoner hvor bunnens egenskaper og vanndybden kan varierer med avstanden. Modellen er basert på strålegangsbergninger og benytter en spesiell metode med sortering og interpolasjon for å finne alle egenstrålene mellom en sender posisjon og et antall mottaker posisjoner som alle må være på samme dyp. Ingen ståler går ned i bunnen, men den akustiske interaksjon med bunnen tas vare på ved å benytte planbølge refleksjonskoeffisienter. Bunnen kan bestå av et fluid sedimentlag over et elastisk halvrom. Modellen tillater at tykkelsen på sedimentlaget samt tettheter og lydhastighetene i sedimentlaget og i det elastiske halvrommet kan variere med horisontalavstanden. Lydhastigheten i sjøvannet kan variere med dybden, men ikke med avstanden.

Modellen beregner strålegangene, gangtidene og amplitudene til alle egenstrålene mellom en gitt senderposisjon og mottaker posisjonene og finner hele frekvensresponsen ved koherent addisjon av bidragene fra alle egenstrålene. Ved å multiplisere frekvensfunksjonen med frekvensspekteret til det utsendte signalet bergenes tidsforløpte og frekvensinnholdet til de mottatte signalene i alle mottakerposisjonene.

Rapporten beskriver modellen og illustrere bruken ved hjelp av en rekke eksempler. Nøyaktighet til stålegangs beregninger og denne modellen i diskuteres og resultatene sammenliknes med resultatene fra andre akustiske forplantningsmodeller basert på bølgetallsintegrasjon og løsningen av den parabolske ligningen.

Contents

1 Introduction

Modeling the acoustic propagation conditions has always been an important issue in underwater acoustics and there exists a vide variety of mathematical/numerical models based on different approaches. The most common models are based on normal modes (Jensen and Ferla, 1979), the parabolic equation (Collins, 1993, 2001) and models based on the wave number integration technique (Schmidt, 1987, 1993); all these models have been extended to deal with range dependent problems. Ray tracing models, which are the oldest and simplest class of models, have for some time been consider outdated as compared with the more sophisticated models mentioned above. However, in recent years there seems to be a new interest for ray tracing models, also for long range, low frequency applications. There may be several reasons for this. Firstly, ray trace models may be more accurate than commonly believed, also for low frequency applications. Secondly, representing the sound field by rays gives a more physical description that is easier to understand and interpret than other types of field descriptions. Finally, ray tracing models are efficient since the main calculation of ray trajectories is independent of frequency; the frequency enters only through the interaction with the boundaries, sea surface and sea floor, and can be introduced separately.

For these reasons we have developed a forward acoustic propagation model, named PlaneRay based on ray tracing. An essential feature of this model is a unique sorting and interpolation routine, and the model has proved to be efficient in determining eigenrays also for range dependent environments. The bottom is modeled with plane wave reflection coefficient, and in principle any number of elastic or acoustic layers can be modeled. In the present implementation the bottom has a fluid sedimentary layer over an elastic half space and the layer thickness and the material properties are allowed to be range dependent. The sound speed profile in the water can only be a function of depth and is not allowed to vary in the horizontal direction. The effects of a layered bottom are included with plane wave reflection coefficients and rays are only traced to the water-sediment interface and not into the bottom. Figure 1 shows the general propagation problem that can be modeled with PlaneRay. The receivers are located on a horizontal line in the water.

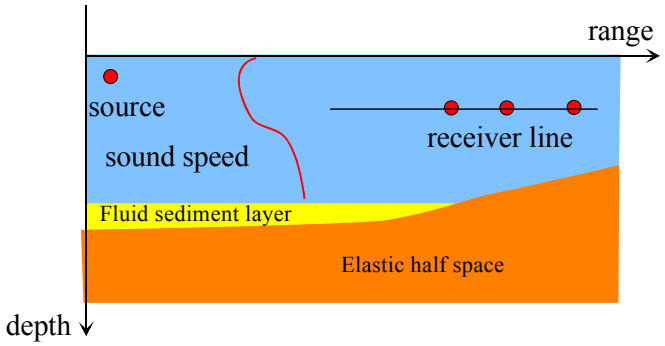

Figure 1. The PlaneRay model computes the received field from a source at receivers located on a horizontal line. The sound speed profile is only function of depth. The bottom can be a fluid sedimentary layer over an elastic half space and both can be range dependent.

Figure 2 shows two typical scenarios with geophysical models of the bottom that can be modeled with the PlaneRay model. The bottom is characterized with a sediment layer over hard bedrock. In some cases the sea bed is almost horizontal (upper), in other areas with intrusions of hard rocks all the way up the water interface (lower). In this case the sound speed is approximately constant with depth and range

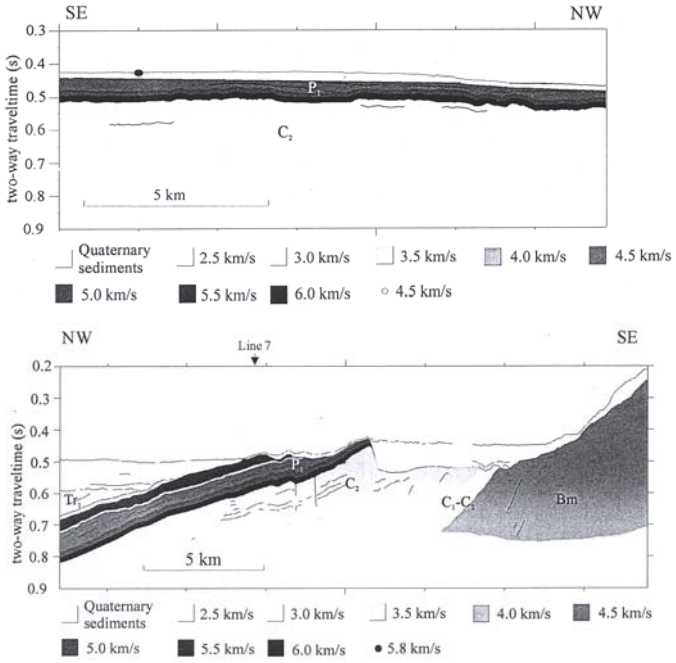

Figure 2. Geoacoustic model for two relevant areas that can be modelled with the PlaneRay model. The bottom is characterized with a sediment layer over hard bedrock. In some cases the sea bed is almost horizontal (upper), in other areas with intrusions of hard rocks all the way up the water interface (lower). The sound speed is approximately constant with dept and range.

The results of a typical application of the model are illustrated in Figure 3.The input data is the sound speed profile and the topography and the geoacoustic model of the bottom. The program determines the trajectories, that travel times and amplitudes of all the eigenrays connecting a source position to one or more receiver positions and add coherently the contributions to produce the transmission loss as function of frequency and range, or the time response of the received signal at several receiver stations.

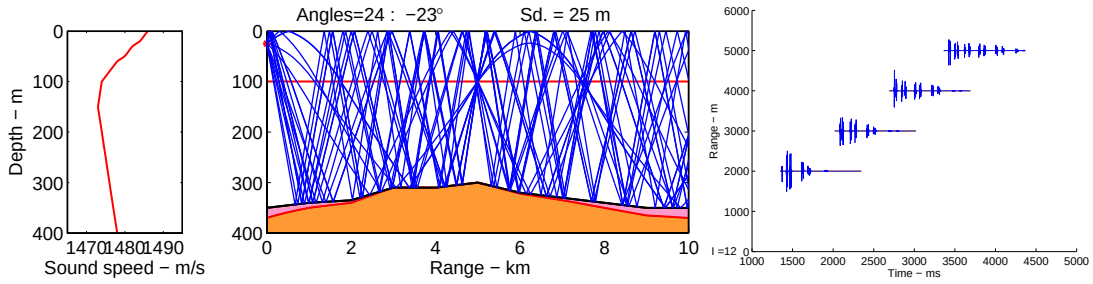

Figure 3. *Illustration of the PlaneRay model. Left: The sound speed profile. Centre: The scenario with propagation to a distance over 10 km where the water depth changes gradually with range and where the bottom has a sedimentary layer of varying thickness over a solid half space. The program determines the trajectories, travel times and amplitudes of all the eigen rays connecting a source position to one or more receiver positions and adds coherently the contributions to produce the transmission loss as function of frequency and range or the time response of the received signal at several receiver stations (right).*

The use of ray tracing for propagation modeling is not new or original and many such models have been developed and presented in the literature earlier. In particular, we point to articles of Westwood and Vidmar (1987) and Westwood and Tindle (1987) where ray tracing is applied for time- series simulation of shallow water propagation with a homogeneous fluid bottom. The main difference is that the PlaneRay can handle range-dependent bottom topography and structure, but no rays are traced into the bottom as is done with the model of Westwood and Vidmar (1987). In a more recent paper Stotts et al. (2004) reported on modelling transmission loss in range dependent environments using ray tracing. Although the principle of using ray theory is the same as used in PlaneRay, the implementations are very different, in particular is the algorithm for finding the eigenrays very different.

In this paper we first describe the PlaneRay model and then present some results from testing and comparison with other models for both range independent and range dependent scenarios.

2 Model description

The algorithm can be considered as having three stages:
(1) The initial ray tracing using a large number of rays to map out the entire sound field.
(2) Sorting and interpolation to determine the trajectories and the ray history of the eigenrays connecting the source to the receivers.
(3) Synthesis of the acoustic field in frequency domain by coherently adding the contributions of the eigenrays, and calculation of the full-waveform time responses by Fourier transformation.

2.1 Initial ray tracing

The input information is the range dependent bathymetry, a sound speed profile and the source location and the receiver depth. The initial ray tracing is done by launching a relative large number of rays, (typically 1000 rays) with angles selected to cover the entire space between a fixed source location and out to receiver on a horizontal line at the specified receiver depth. For each ray, the model computes the ranges and the travel times to the locations where the ray intersects the receiver depth, and records the locations and the angles for reflection from the bottom and the surface. All this information is stored and used in the following stages. Notice that the rays are not traced into the bottom and that both the sound speed profile and the bathymetry are fixed; therefore the ray tracing is only executed once for each site.
The theory of acoustic waves (Jensen et al. 1993 and Clay and Medwin, 1977) is well known and shall not be developed here. The implementation used in the PlaneRay model is to divide the water column into a large number of layers with the same thickness Δz. Within each layer, the sound speed is approximated with a straight line so that, in the layer $z_i<z<z_{i+1}$, the sound speed is taken to be

$$c(z) = c_i + (z - z_i) g_i \quad . \tag{1}$$

where c_i is the sound speed at depth z_i, and the sound speed gradient in the segment is g_i. Since the sound speed in each of these layers has a constant gradient, the ray in each layer follows a circular arc; the arc's radius of curvature $R_i(z)$ is given by the local sound speed gradient $g_i(z)$ and the ray parameter ξ,

$$R_i(z) = -\frac{1}{\xi g_i(z)} \quad , \tag{2}$$

The ray parameter is defined as:

$$\xi = \frac{\cos\theta_s}{c(z_s)} \tag{3}$$

where θ_s is the initial angle of the ray's trajectory at the source depth z_s and $c(z_s)$ is the sound speed at the source depth. After traveling through the layer from z_i to z_{i+1} the ray's range increment is

$$r_{i+1} - r_i = -R_i \left(\sin\theta_{i+1} - \sin\theta_i \right), \tag{4}$$

which also can be written in the form

$$r_{i+1} - r_i = \frac{1}{\xi g_i} \left[\sqrt{1 - \xi^2 c^2(z_{i+1})} - \sqrt{1 - \xi^2 c^2(z_i)} \right] \quad . \tag{5}$$

The local sound speed gradient is approximated by

$$g_i = \frac{c(z_{i+1}) - c(z_i)}{z_{i+1} - z_i} \quad . \tag{6}$$

The travel time increment is

$$\tau_{i+1} - \tau_i = \frac{1}{|g_i|} \ln \left(\frac{c(z_{i+1})}{c(z_i)} \frac{1 + \sqrt{1 - \xi^2 c^2(z_i)}}{1 + \sqrt{1 - \xi^2 c^2(z_{i+1})}} \right) \quad . \tag{7}$$

When the water depth varies with distance the ray parameter is no longer constant, but changes with the bottom inclination angle. An incoming ray with angle θ_{in} is reflected to the angle θ_{ref} when the bottom angle is α.

$$\theta_{ref} = \theta_{in} + 2\alpha. \tag{8}$$

Consequently, the ray parameter has to change to

$$\begin{aligned} \xi_{ref} &= \frac{\cos(\theta_{ref})}{c} = \frac{\cos(\theta_{in} + 2\alpha)}{c}, \\ &= \xi_{in} \cos(2\alpha) - \frac{\sqrt{1 - \xi_{in}^2 c^2}}{c} \sin(2\alpha). \end{aligned} \tag{9}$$

The algorithm makes repeated use of Equations (5) and (7), stepping with depth increments Δz in such a way that the new depth z_{i+1} is given by the old depth z_i as

$$z_{i+1} = z_i \pm \Delta z \quad . \tag{10}$$

The plus sign indicates a ray going downwards and the minus sign, a ray going upwards. Evidently the sign has to change when the ray strikes the bottom and the surface, and when the ray goes through a turning point.

The calculation of the trajectories and travel time described above assumes that the ray's curvature is finite, i.e. that the sound speed gradient is non zero and in real life this will always be the case. However, in testing and in some studies it is useful to have the possibility of using a constant sound speed; in such cases Equations (5) and (7) are exchanged with the following equations:

$$r_{i+1} - r_i = \left| z_{i+1} - z_i \right| / \tan\left(\theta_{i+1} \right) \tag{11}$$

$$\tau_{i+1} - \tau_i = \left| z_{i+1} - z_i \right| / \left[c_{i+1} \sin\left(\theta_{i+1} \right) \right] \tag{12}$$

The acoustic intensity is calculated by using the principle that the power within a space limited by a pair of rays with initial angular separation of $d\theta_0$ centered on the initial angle θ_0 will remain between the two rays, regardless of the rays' paths. The acoustic intensity as function of horizontal range, $I(r)$ is according to this principle given by

$$I(r) = I_0 \frac{r_0^2}{r} \frac{\cos\theta_0}{\sin\theta} \left| \frac{d\theta_0}{dr} \right| \quad . \tag{13}$$

By applying Snell's law we can transform Equation (13) into an expression often found in text books,

$$I(r) = I_0 \left(\frac{r_0^2}{r} \right) \left(\frac{c_0}{c} \right) \frac{\cos\theta}{\sin\theta} \left| \frac{d\theta_0}{dr} \right| \quad , \tag{14}$$

The expression of Equations (14) is not valid when the bottom depth varies with range since the ray parameter is then changed by the bottom reflections as given by Equation (9), the intensity is therefore calculate by using Equation (13). Both expressions, Equations (13) and (14), break down at turning points and at caustics. We will later describe how this problem is treated in the model.

The geometrical part of the transmission loss is defined as

$$TL(r) = -10 \cdot \lg\left(\frac{I(r)}{I_0} \right). \tag{15}$$

Note that absorption and losses associated with reflections from the sea bottom or surface are not include, only refraction effects and geometrical spreading is included in the expression of Equation .(15).

A typical plot of range to receiver depth as function of initial launch angle will look as shown in Figure 4. The grouping of angle, range pairs in rather smooth curves are noticeable and this behavior is utilized in the sorting and interpolation scheme.

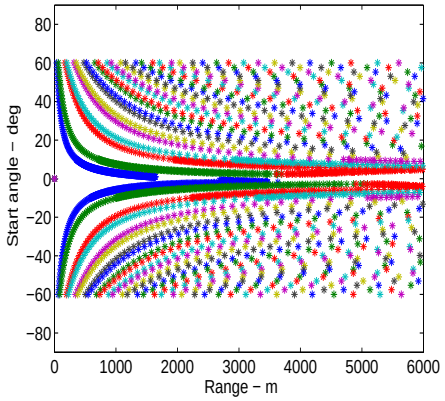

Figure 4. Recording of the ranges to the given receiver depth intersection as function of the rays initial angle resulting from the initial ray tracing.

The first step in the modeling is to apply the algorithm described above to a relative large number of rays spanning the whole range of initial angles that are relevant for the actual studies. For each ray, the trajectory, travel time and the transmission loss are calculated and stored in the computer together with the ray history in terms of number, angle and locations of bottom and surface reflections and turning points. Since the sound speed profile and the bathymetry are supposed to be fixed, and not changed, this ray tracing calculation is only done once for each site.

2.2 Beam displacement

Beam displacement is also implemented in the model as an option. When the incident grazing angle is lower than the critical angle the ray appears to be displaced a certain distance Δl along the interface. The beam displacement is

$$\Delta l = \frac{\partial \delta}{\partial k}. \tag{16}$$

Here δ is the phase angle of the reflection coefficient for the interface between the water (0) and the bottom (1) for angles lower than the critical angle (Tindle and Bold, 1981)

$$\delta = 2\tan\left(-i\frac{\rho_0\gamma_1}{\rho_1\gamma_0}\right). \tag{17}$$

The beam displacement therefore can be expressed as

$$\Delta l = 2k\frac{\rho_0\rho_1(\gamma_0^2+\gamma_1^2)}{\gamma_0\gamma_1(\rho_1^2\gamma_0^2+\rho_0^2\gamma_1^2)}. \tag{18}$$

The difference in propagation time between a beam displaced at the bottom and a beam reflected directly from the bottom is

$$\Delta t = \frac{\Delta l}{c_0}(1-\cos\theta_0). \tag{19}$$

In these equations the horizontal wave number, γ_0 and γ_1 are the vertical wave numbers and ρ_0 and ρ_1 are the densities of the water and the bottom medium respectively. The beam displacement of Equation (18) and the difference in propagation time of Equation (19) are functions of frequency and valid only for the half-space model with a vertical homogeneous bottom. In the PlaneRay model the beam displacement is introduced in the initial ray tracing for one frequency specified by the user and can therefore only be used for narrow frequency band signals around that frequency. Figure 5 shows the results of Equations (18) and (19) using the parameters c_0=1500 m/s c_1=1700 m/s, ρ_0 =1000 kg/m^3 and ρ_1 =1500 kg/m^3. Note that the beam displacement, according to Equation (18) and Figure 5, increases sharply in the vicinity of the critical angle. This indicates a limitation of the validity of this approach

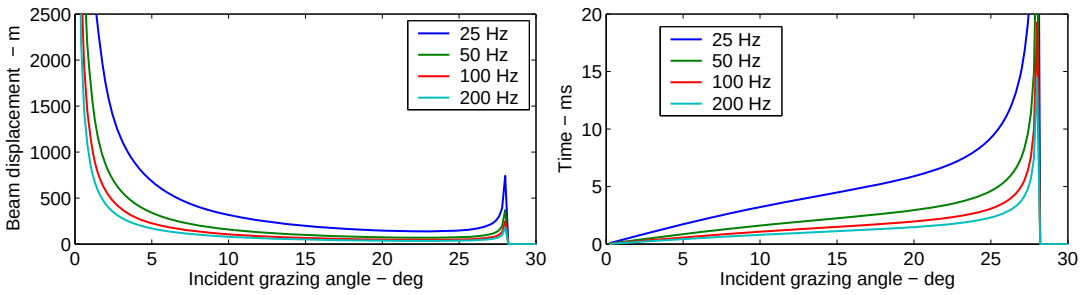

Figure 5. *Beam displacement (left) and travel time increase (right) as function of incident grazing angle. Calculated by Equations (18) and (19) for the frequencies of 25, 5, 100, 200 Hz and the parameters c_0=1500 m/s c_1=1700 m/s ρ_0 =1000 kg/m^3, and ρ_1 =1500 kg/m^3.*

2.3 Eigenray determinations

The next step is to determine the eigenrays and their trajectories. The approach used in PlaneRay is based on interpolation on the results of the initial ray tracing. However, the interpolation has to be done on rays that have same type of ray history. This consideration is illustrated in Figure 6 which shows a simple example of ray tracing with constant water depth and sound speed.

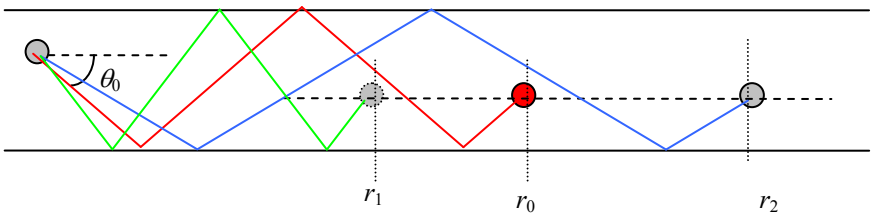

Figure 6. *An eigenray to the receiver at range r_0 is found by interpolating between the two rays arriving at the same receiver depth at ranges r_1 and r_2.*

The figure shows three ray paths from the source to reach three receivers at the same depth at different ranges. All the three rays have gone through one reflection from the surface and two reflections from the bottom. The two rays intersecting the receiver depth at ranges r_1 and r_2 are the two rays from the initial ray tracing and the desired ray is the ray with start angle θ_0 that is reaching the target at range r_0. Notice that all the rays have the same number of reflections from the surface (one) and the bottom (two). Therefore the relation between initial angle θ_0 and receiver range can be expected to follow a reasonable smooth curve amendable to interpolation. The generalization of this example to any number of surface and bottom interactions and inclusions of rays with upper or lower turning points is implemented in the program. In the special the case of a constant sound speed *c(z) = constant* there will be 5 classes of arrivals and these are the classes 0, 1, 2, 3 and 4 shown in Table 1. The example of Figure 6 corresponds to Class 4 with n=2.

With a depth dependent sound speed profile there can be additional classes with upper and lower turning points. These are labeled Class 5, 6, 7 for rays going through upper turning points, in situations with negative sound speed gradients, and Class 8, 9, 10 for rays going through lower turning points for positive sound speed gradients. The classes 14, 15, 16 and 17 are for rays going

through one or more upper and lower turning points without striking the bottom. In range dependent environments with varying water depths there may be other combinations than the ones defined in Table 1. In such cases the user has to define the additional classes with the desired combinations of the numbers of upper and lower turning points and number of surface and bottom reflections.

Figure (7) shows an example of the interpolation scheme to determine the eigenrays to reach a receiver at a specific range, in the example of Figure 7 the range is 1000 meter and we find 8 eigenrays with angles with values -19.3°, -16.7°, -8.5°, -5.7°, 2.9°, 5.7°, 14.1°, 16.7°. It is easy to verify that these values are correct.

Table 1

Class	*Bottom*	*Surface*	
Class 1	*0*	*0*	*Direct ray*
Class 2	*n-1*	*n*	*Negative start angle*
Class 3	*n*	*n*	*Negative start angle*
Class 4	*n*	*n*	*Positive start angle*
Class 5	*n*	*n-1*	*Positive start angle*
Class	*Bottom*	*Upper tuning points*	
Class 6	*n*	*n+1*	*Negative start angle*
Class 7	*n*	*n*	*Negative start angle*
Class 8	*n*	*n*	*Positive start angle*
Class 9	*n+1*	*n*	*Positive start angle*
Class	*Surface*	*Lower turning points*	
Class 10	*n+1*	*n*	*Negative start angle*
Class 11	*n*	*n*	*Negative start angle*
Class 12	*n*	*n*	*Positive start angle*
Class 13	*n*	*n+1*	*Negative start angle*
Class	*Upper turning points*	*Lower turning points*	
Class 14	*n*	*n-1*	*Negative start angle*
Class 15	*n*	*n*	*Negative start angle*
Class 16	*n*	*n*	*Positive start angle*
Class 17	*n-1*	*n*	*Positive start angle*

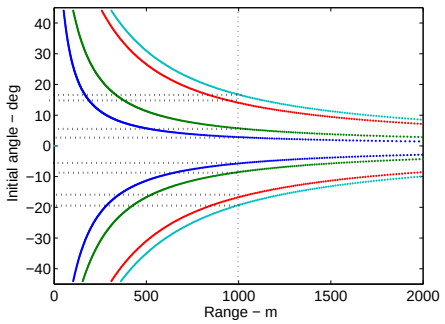

Figure 7. Ranges to the given receiver depth intersection as function of the rays initial angle resulting from the initial ray tracing.

2.4 Turning points and caustics

Equation (13) predicts infinite intensity under two conditions, when $\theta=0$ and when $dr/d\theta_0=0$. The first condition signifies a turning point where the ray path becomes horizontal; the second condition occurs at points where an infinitesimal increase in the initial angle of the ray produces no change in the horizontal range traversed by the ray. In both cases there is focusing of energy by refraction where infinite amplitude is predicted by classical ray theory.
This section illustrates how the model handles caustics and turning points by showing a simple example where sound speed is increasing monotonically with depth according to

$$c(z) = c_0 + gz\,. \tag{20}$$

With the values c_0=1475 m/s and g=0.03 s^{-1}.
Figure 8 shows the rays with initial angles from 0.1°to 6° at 0.1° intervals. The two dashed lines are the caustics for ray having been through one (m=1) and two (m=2) turning points respectively. The caustics are calculated by the method outline in the book by Officer (1958).

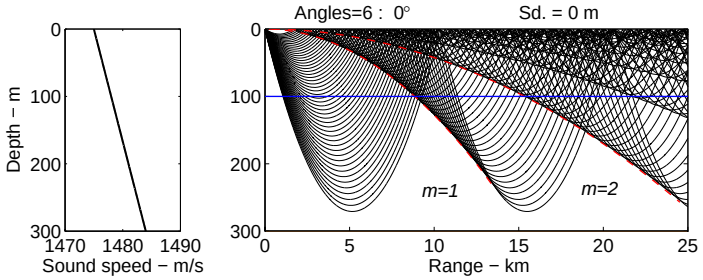

Figure 8. Example of turning points and caustics. The figure shows ray paths for rays with initial angle from 0.1°to 6° at 0.1° intervals. The caustics are shown with dashed lines for m=1 and m=2 turning points.

According to Snell's law the turning points at the 100 m depth occur when the initial angle equals arcos[c(0)/ c(100)], in this case when θ_0 = 3.65° at ranges of 2.97 km, 9.65 km, 15.51 km and 22.23 km.

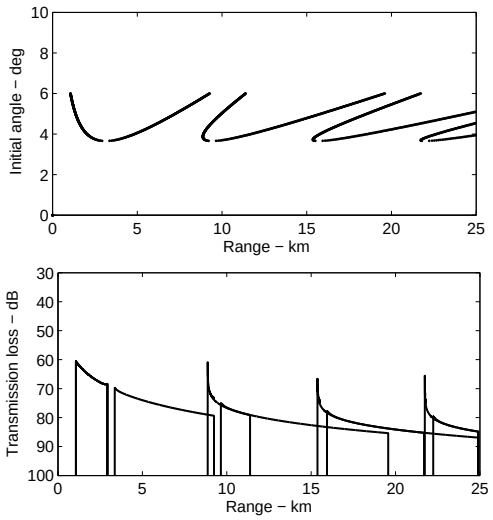

Figure 9. Upper: Range to a receiver at 100 m depth as function of initial angle θ_0 between 0 ° and 6 °Lower: Ray amplitudes to receivers at 100 m depth as function of range for the same angles as shown in the left-hand figure.

The upper part of Figure 9 shows the range to a receiver at 100 m depth as function of initial launch angle θ_0. The lower panel shows the geometrical transmission loss as function of range for some of the multi path contributions. Notice the small gaps gaps in the transmission loss curves at the ranges of the turning points, this is most noticeable at 2.97 km. The caustics are where $dr/d\theta_0 = 0$ and can, in both plots, be seen at the ranges 8.9 km, 15.4 km and 21.7 km. The model produces very strong fields at ranges near and beyond the caustics and total shadow zones for shorter ranges near the caustics. The behaviours at turning points and at caustics are as anticipated for classical ray theory. Methods to improve the estimates at caustics and turning points are found in the literature, for instance Jensen et al. (1993), but presently not implemented in the model.

2.5 Synthesis of the sound field

The received sound field is synthesized by coherent additions of the contributions of all the eigenrays. No rays are traced into the bottom and the effects of a layered bottom are described entirely by plane ray reflection coefficients. In the current implementation the bottom is modelled with a fluid sedimentary layer over a homogeneous solid half space. The thickness of the layer and the parameters of the layer and the half space can vary with range in any manner specified by the user.

The bottom reflection coefficient of this bottom is

$$R_b = \frac{r_{01} + r_{12} \exp\left(-2i\gamma_{p1} D\right)}{1 + r_{01} r_{12} \exp\left(-2i\gamma_{p1} D\right)} \tag{21}$$

where γ_{p1} is the vertical wave number for sediment layer and D is the thickness of the sediment layer. The reflection coefficient between the water and the sediment layer, r_{01}, is given as

$$r_{01} = \frac{Z_{p1} - Z_{p0}}{Z_{p1} + Z_{p0}}, \tag{22}$$

and r_{12} is the reflection coefficient between the sediment layer and the solid half space,

$$r_{12} = \frac{Z_{p2}\cos^2 2\theta_{s2} + Z_{s2}\sin^2 2\theta_{s2} - Z_{p1}}{Z_{p2}\cos^2 2\theta_{s2} + Z_{s2}\sin^2 2\theta_{s2} + Z_{p1}} \tag{23}$$

In Equations (15) and (16) Z_{ki} is the acoustic impedance for the compressional ($k = p$) and shear ($k = s$) waves in water column ($i = 0$), sediment layer ($i = 1$) and solid half-space ($i = 2$), respectively. θ_{s2} is the transmitted grazing angle for the shear wave in the solid half-space. Figure 10 shows an example of the bottom loss as function of angle and frequency for a sediment layer with the thickness $D = 5$ m, density 1500 kg/m^3 and sound speed 1700 m/s over a homogeneous half space with density 2500 kg/m^3 and compressional sound speed 4700 m/s and shear speed 2200 m/s. Notice the anomalous high reflection loss at angles around 20 degrees and 200 Hz as well as zero degrees and 75 Hz, this will be discussed later.

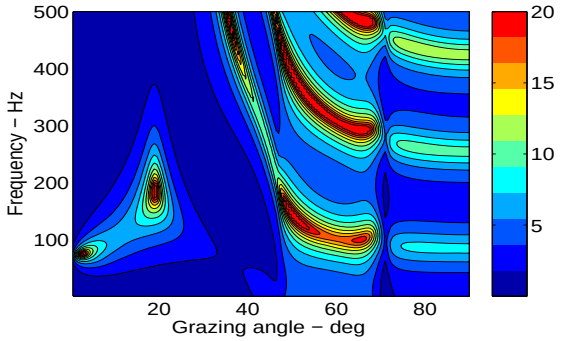

Figure 10. Bottom reflection loss for a sediment layer with thickness D = 5 m, density 1500 kg/m^3 and sound speed 1700 m/s over a homogeneous half space with density 2500 kg/m^3, compressional sound speed 4700 m/s and shear speed 2200 m/s.

3 Case studies

This section presents the result of testing the model and comparing the results with other propagation models. Other tests of the Plane Ray model have been done by Smedsrud and Tollefsen at FFI, (Smedsrud and Tollefsen 2007)

In the tests and examples to be presented here, some will show the time responses and in all these cases the source signal is a short Ricker pulse with time signature and frequency spectrum as shown in Figure 11.

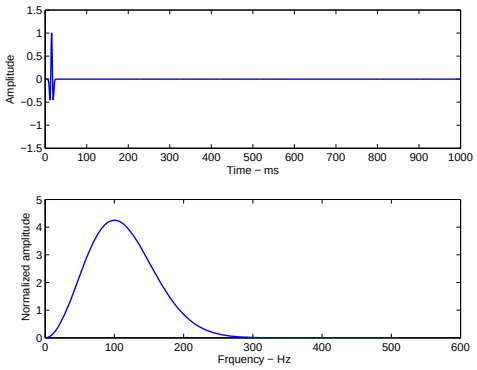

Figure 11. Source signal (upper) and its frequency spectrum (lower) used in the calculation of the time responses.

3.1 Range independent cases

3.1.1 The Pekeris' wave guide

We present results calculated by PlaneRay model for range independent cases and compare with the results of the wave number integration model OASES (Schmidt, 1987, 1993). The first case is the so called Pekeris' case (Pekeris, 1948) with water depth 100 m, layer thickness D =0. The sound speed and density in water are constants, respectively c_0 = 1500 m/s ρ_0 =1000 kg/m^3 and the sound speed of the bottom is 1700 m/s and the density is 1500 kg/m^3, the absorption in the bottom is 1 dB/ wavelength.

Figure 12 shows the transmission loss as function of range and frequency and the time response at a number of receivers out to the range of 20 km. In the time plots we have added the line that corresponds to rays that are striking the bottom with the critical angle. The equation of this line for reduced time t_{red} versus range r is

$$t_{red} = \frac{r}{c_0}\left(\frac{1}{\cos\theta_{crit}} - 1\right). \qquad (24)$$

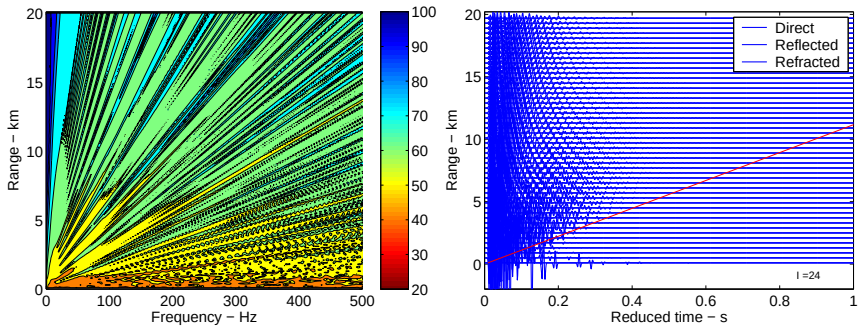

Figure 12. Frequency and time response of a Pekeris' wave guide where the bottom sound speed is 1700 m/s, the density is 1500 kg/m^3. Left: Transmission loss as function of range and frequency. Right: Time response for a number of receivers with distances from 100 meter to 20 km from the source. The source signal is a short transient (Ricker wavelet).

Figure 13 shows the transmission loss as function of range for the selected frequencies of 25, 50, 100 and 200 Hz compared with the results using OASES for the same case. For the lowest frequency, 25 Hz, the agreement is rather poor, but for the higher frequencies the PlaneRay results agree quite well with the OASES results.

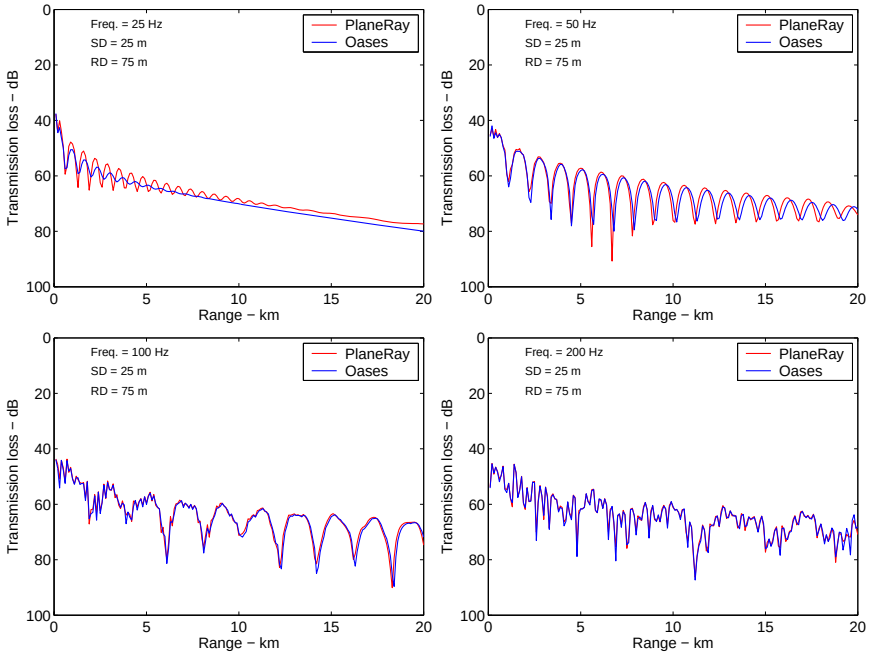

Figure 13. Comparison of the transmission loss as function of range for different frequencies by PlaneRay (red line) and OASES (blue line) for Pekeris' wave guide where the bottom sound speed is 1700 m/s, the density is 1500 kg/m^3.

The oscillations in transmission loss with range are caused by mode interference. Notice that there is shift in the interference patterns of the two results, most pronounced for low frequencies and long ranges. This can to some extent be corrected by beam displacement to be discussed next. The ray approximation to the solution of the wave equation is, by common definition, considered valid for frequencies higher than the frequency where the water depth is two times the

wavelength. Since the water depth in this example is 100 meter this definition gives a lower frequency limit of 30 Hz which is in agreement with we have observed in Figure 13.

3.1.2 Correction for beam displacement

The comparison with the OASES results in Figure 13 shows that the oscillations in the transmission loss with range are a little out of phase and shifted in range. In order to explain this we redo the ray tracing and apply the beam displacement option of the model, implemented with Equations (18) and (19). As the beam displacement is frequency dependent, we have to choose a particular frequency and in this case we chose 50 Hz. The beam corrected transmission loss curves are shown in Figure 14

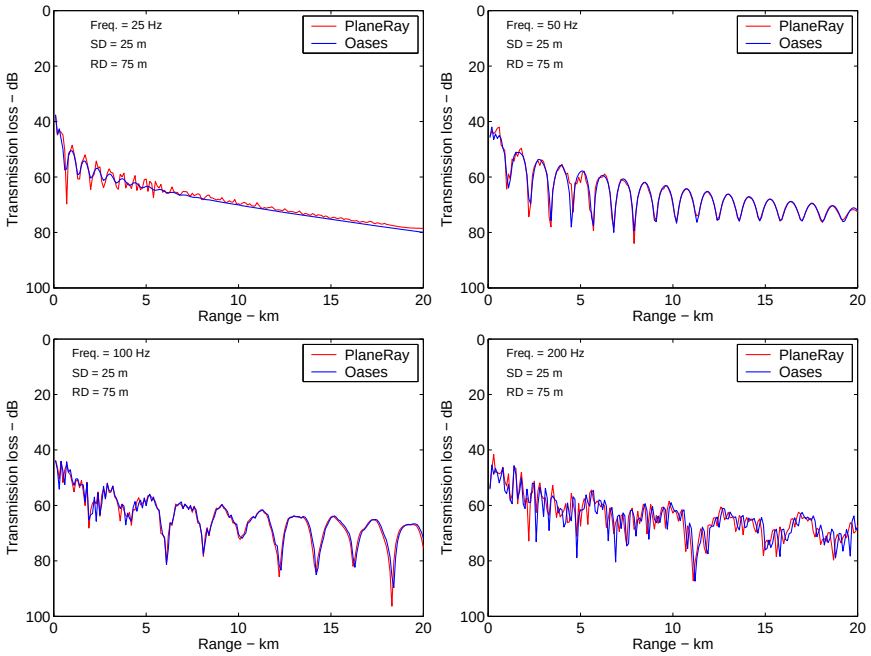

Figure 14. Transmission loss as function of range for the frequencies 25, 50, 100, 200Hz. Calculated with beam displacement optimized for 50 Hz.

The agreement for the frequency of 50 Hz is considerably improved, but there this an increased level of numerical noise at the shortest distances. For 100 Hz and 200 Hz the agreement with OASES is poorer, which is as expected since the beam displacement in this case is optimized and calculated for 50 Hz.

3.1.3 Homogeneous slow speed sediment bottom

The next case is with a homogeneous mud bottom with a sound speed of 1450 m/s and density of 1200 kg/m^3. These is a situation that causes intromission of rays with grazing angles at the bottom approximately 23.5°and consequently very high bottom reflection loss for steeper angles. This shown in Figure 15 and the ray tracing results are in excellent agreement with the OASES results for all frequencies.

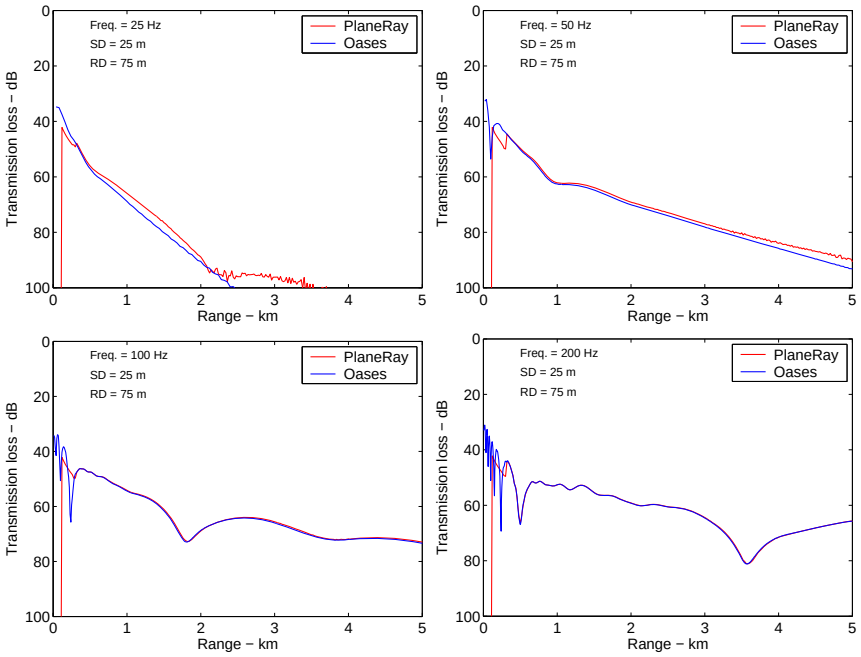

Figure 15. Comparison of the transmission loss as function of range for different frequencies by PlaneRay (red line) and OASES (blue line) for Pekeris' waveguide with a low sound speed mud bottom. The sound speed of the sediment is 1450 m/s and the density is 1200 kg/m^3.

3.1.4 Elastic homogeneous bottom

We consider the same wave guide, but with an elastic homogeneous bottom. The water depth is 100 m with constant sound speed in the water of 1500 m/s. The source depth is 25 m and the receiver depths are 75 m. The bottom is an elastic half-space with parameters c_p=3000 m/s, c_s=500 m/s, density 1800 kg /m^3, and both waves with attenuations of 0.5 dB per wavelength. Figure 16 shows the frequency and time responses, and Figure 17 compares the transmission loss as function of range for the frequencies of 25, 50, 100 and 200 Hz with the results produced by the OASES model. Again, the ray trace results compare very well with the OASES results.

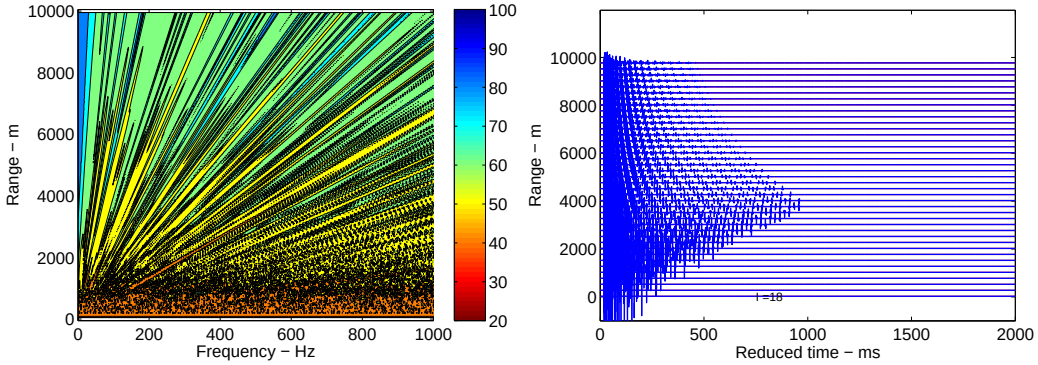

Figure 16. Frequency and time response of a Pekeris' wave guide with a homogeneous solid bottom with compressional speed 3000 m/s and shear speed 500 m/s.
Left: Transmission loss as function of range and frequency.
Right: Time responses for a number of receivers with distances from 100 meter to 10 km from the source. The source signal is a short transient (Ricker wavelet).

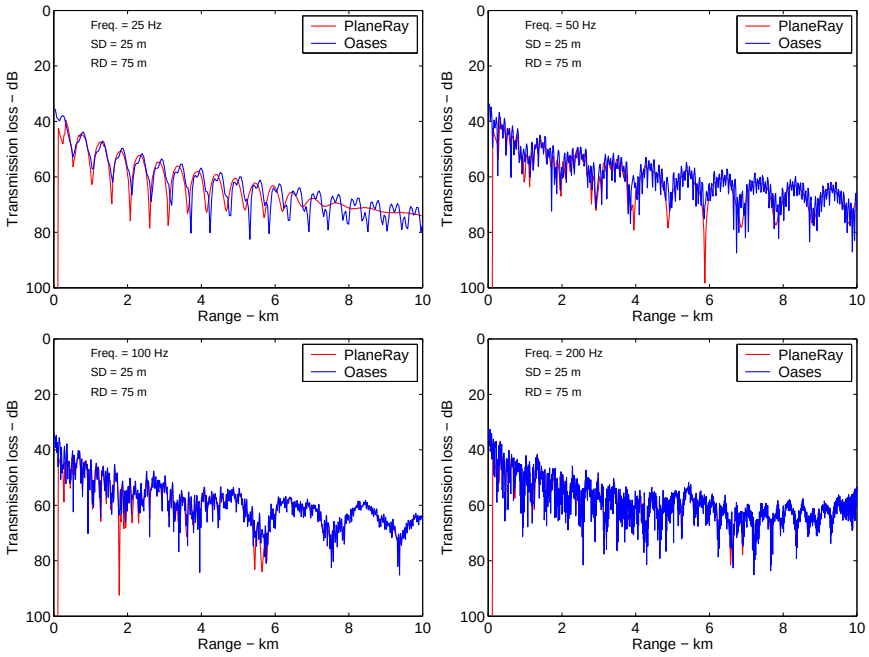

Figure 17. Comparison of the transmission loss as function of range for different frequencies by PlaneRay (red line) and OASES (blue line) for Pekeris' waveguide with a homogeneous solid bottom with compressional wave speed 3000 m/s and shear wave speed 500 m/s.

3.1.5 Modelling the effect of layered bottoms

As stated before, the model does not trace rays down in the bottom and the effect of a deeper interface is entirely modeled through the bottom reflection coefficient. It is therefore interesting to compare the PlaneRay results with a model that treats a layered bottom correctly. We consider the structure shown in Figure 18 with three different cases of bottom properties. In all cases the water depth is $H = 100$ m and the layer thickness considered are $D = 2$, 5 and 10 m. The bottom parameters for the three different cases are given in Table 2.

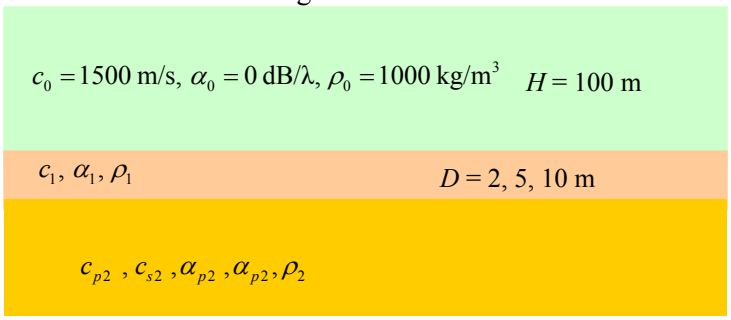

Figure 18. The bottom structure for the CASE 1, 2 and 3. The parameter values given in the figure are the same for all cases, the other parameters are given in Table 2.

Table 2

CASE	Description	Sediment Sound speed c_1 Density ρ_1 Attenuation α_1	Solid half-space Sound speed c_{p2} Density ρ_2 Attenuation α_{p2}	Solid half-space Shear speed c_{s2} Shear attenuation α_{s2}
1	Mud layer over	1450 m/s	1800 m/s	0

	sediment	1500 kg/m^3 1.0 dB/wavelength	2000 kg/m^3 1.0 dB/wavelength	0
2	Sediment layer over bedrock, high shear speed	1700 m/s 1500 kg/m^3 1.0 dB/wavelength	4700 m/s 2500 kg/m^3 0.5 dB/wavelength	2200 m/s 0.5 dB/wavelength
3	Sediment layer over bedrock, low shear speed	1700 m/s 1500 kg/m^3 1.0 dB/wavelength	4700 m/s 2500 kg/m^3 0.5dB/wavelength	2000 m/s 0.5 dB/wavelength

3.1.6 Mud layer over sediment

In the first example of CASE 1 in Table 2, the bottom has a 5 meter thick mud layer with the very low sound speed of 1450 m/s and density 1200 kg/m^3, over a infinite half space with speed 1800 m/s and density 2000 kg/m^3. In Figure 19 the calculated transmission loss using the PlaneRay model and the OASES model are compared for the frequencies of 50, 100, 150 and 200 Hz. The agreement is quite good, especially for the higher frequencies.

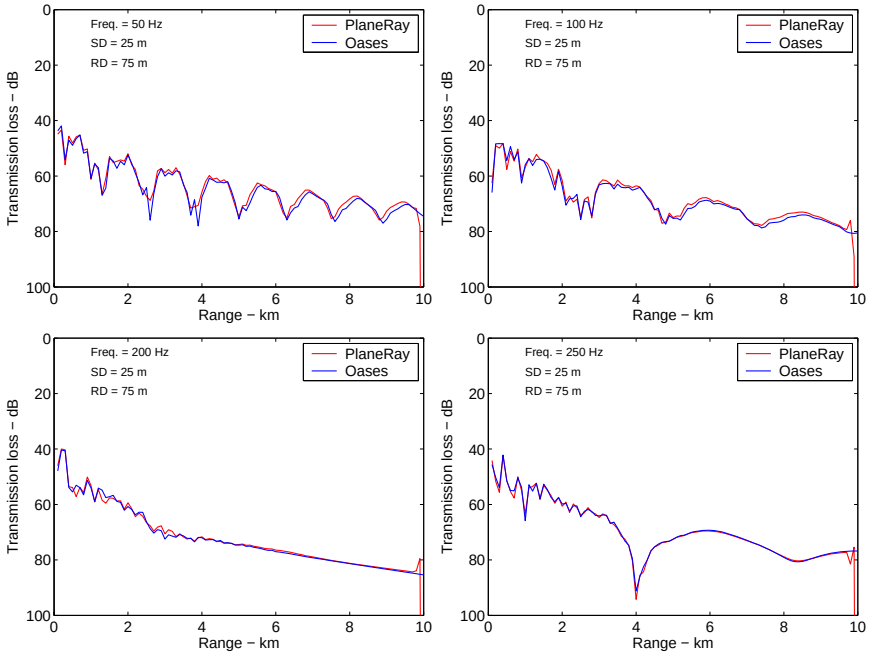

Figure 19. Transmission loss as function of range for the frequencies of 50, 100, 200 and 250 Hz for CASE = 1 in Table 2. The red curves are from the ray trace model, the blue curves are the OASES results.

3.1.7 Fluid sediment layer over hard bedrock

The case with a sediment layer over hard bedrock is particularly interesting because this can result in abnormal high transmission loss for certain combinations of bottom parameters and frequencies. In the following we shall illustrate this effect by a number of examples and, in the same time, compare the ray tracing results with calculation using OASES.

The first example is CASE 2 of Table 2 where there is a 5 meter thick sediment layer over a hard subspace with compressional wave speed of 4700 m/s and shear speed of 2200 m/s. All parameters are specified in Table 2. The left part of Figure 20 shows the time responses for a

number of ranges up to 10 km and the right hand plot shows the frequency domain results in the form of transmission loss as function of range and frequency.

We comment first on the time responses in left panel of Figure 20. The red lines correspond to angles at the surface of 5°, 10° and 25°. A significant feature of the time response is the strongly reduced amplitudes of the arrivals between the two lines representing 5° and 25°. This indicates that the amplitude of the rays hitting bottom at angles between 5° and 25° suffer a significant higher bottom reflection loss.

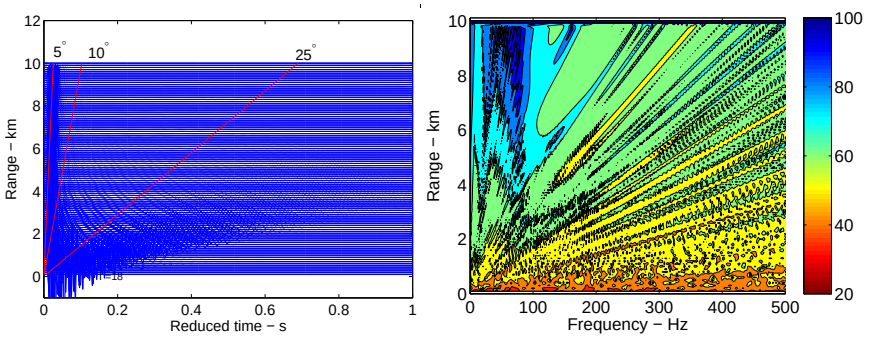

Figure 20. Time responses as function of range (left), and transmission loss as function of range and frequency (right). Sediment layer with thickness 5 meter over hard bedrock with shear speed 2200 m/s. The red lines correspond to angles of 5°, 10° and 25°.

Figure 21 shows the transmission loss as function of range for the selected frequencies of 25, 50, 100 and 200 Hz. And the corresponding results of the OASES model. The agreements are quite good for the higher frequencies, but poorer at lover frequencies, as we have seen before. Notice that both OASES and PlaneRay predict significantly higher transmission loss for 100 Hz than for 200 Hz.

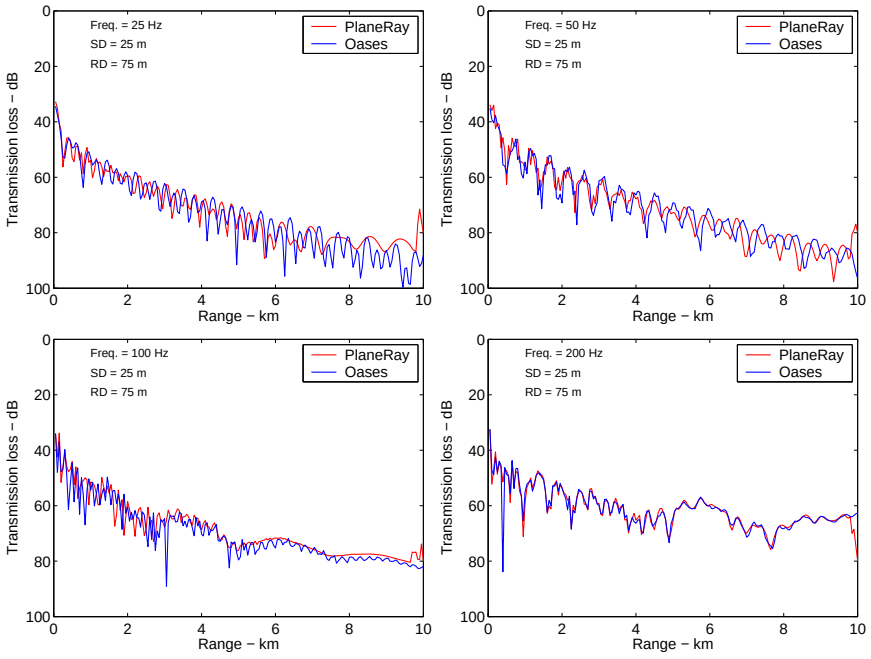

Figure 21. Transmission loss as function of range for the frequencies of 25, 50, 100 and 200 Hz. The bottom has a 5 meter sediment layer over a hard-rock half-space with shear speed of 2200 m/s.

In the calculation of results of Figures 20 and 21, we have used the same parameters as we used to generate the frequency and angle representation of the bottom reflection coefficient shown in Figure 10. Note the triangle-shaped plateau of high reflection loss at angels lower than 20° with two peaks at 80 Hz and 200 Hz. This high reflection loss that may occur for certain combinations of bottom parameter values have been discussed in Hovem and Kristensen (1992), Tollefsen (1989) and by Ainslie (2003) and will not be discussed here. We will however demonstrated the sensitivity by considering the situations where the shear speed in the elastic half space is 2000 m/s and not 2200 m/s, all the other parameters being the same. The new results are shown in Figure 22 and 23

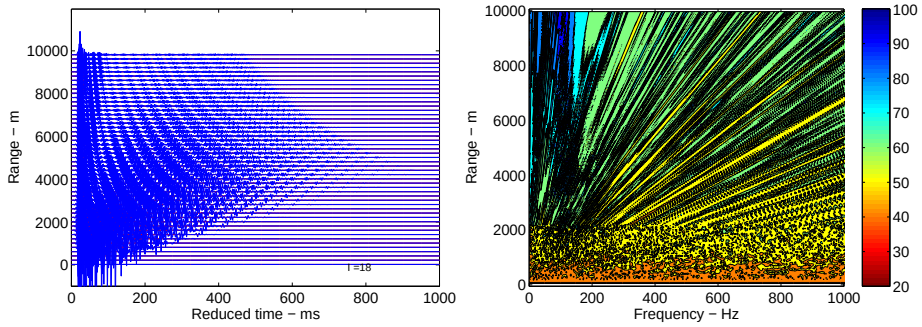

Figure 22. Time responses as function of range (left) and transmission loss as function of range and frequency (right). This case has a sediment layer with thickness 5 meter over hard bedrock with shear speed 2000 m/s.

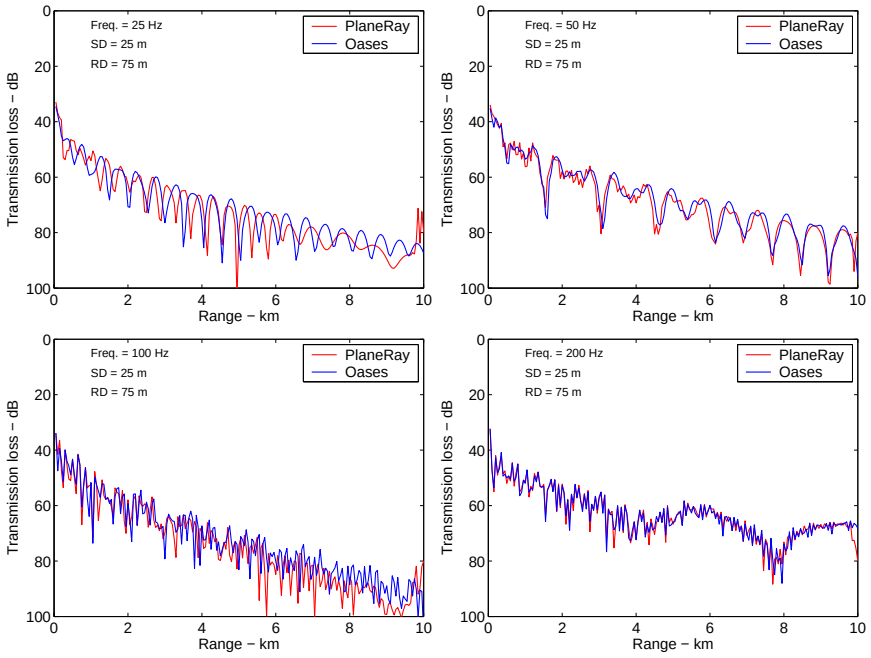

Figure 23. Transmission loss as function of range for the frequencies of 25, 50, 100 and 200 Hz for the case with a sediment layer with thickness 5 meter over hard bedrock with shear speed 2000 m/s.

We complete this study of transmission loss anomalies by considering the same two other cases with the same bottom properties as in used in Figures 21, but with different layer thicknesses. The results are shown in Figure 24 for a layer thickness of 2 m and in Figure 25 for a layer thickness of 10 m. In both cases the results compare very well with OASES, except for the lowest frequency of 25 Hz.

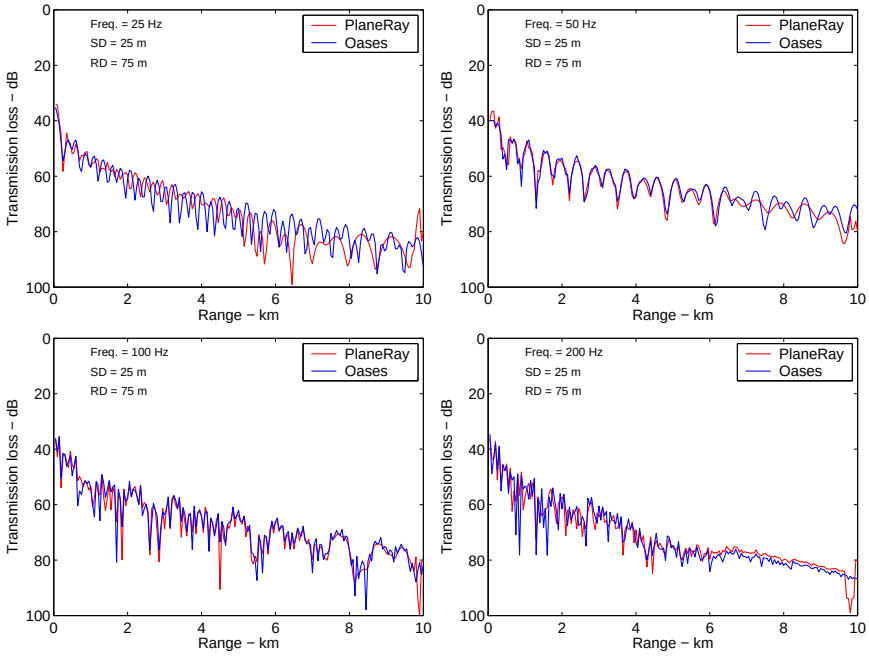

Figure 24. Transmission loss as function of range for the frequencies of 25, 50, 100 and 200 Hz for the case with a 2 meter sediment layer over hard bedrock with shear speed 2200 m/s.

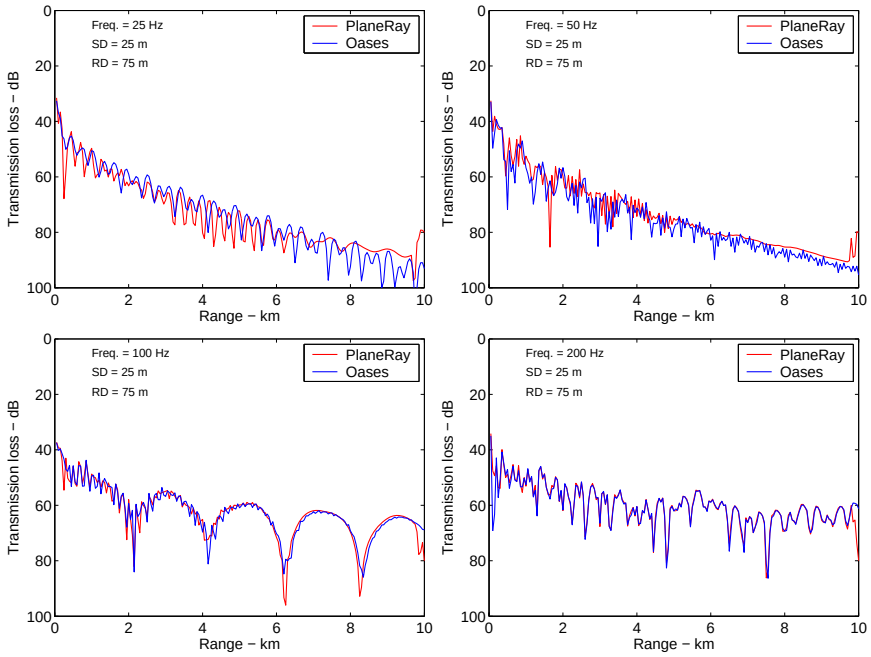

Figure 25. Transmission loss as function of range for the frequencies of 25, 50, 100 and 200 Hz for the case with a 10 meter sediment layer over hard bedrock with shear speed 2200 m/s.

3.2 Positive and negative sound speed gradients

In this section we study how the PlaneRay code is handling turning rays, crossing rays and caustics and we do that by using a linear sound speed profile with

$$c(z) = 1495 - 0.04 \cdot z. \tag{25}$$

The water depth is again 100 m and the source depth is 25 m with the receivers located on a line at 75 m depth out to a distance of 10 km. The bottom is model as fluid half-space with sound speed 1700 m/s, density 1500 kg/m^3, and the absorption is 1 dB per wavelength.
Figure 26 is an illustration of the ray paths and the calculated geometrical transmission loss for this case. The upper part of the figure shows the sound speed profile (left) which has a constant negative gradient (Equation (25)), the upper right part of the figure shows the trajectories of 10 rays in the angle interval of ± 5°. The lower part of the figure shows the calculated geometrical transmission loss as function of range.

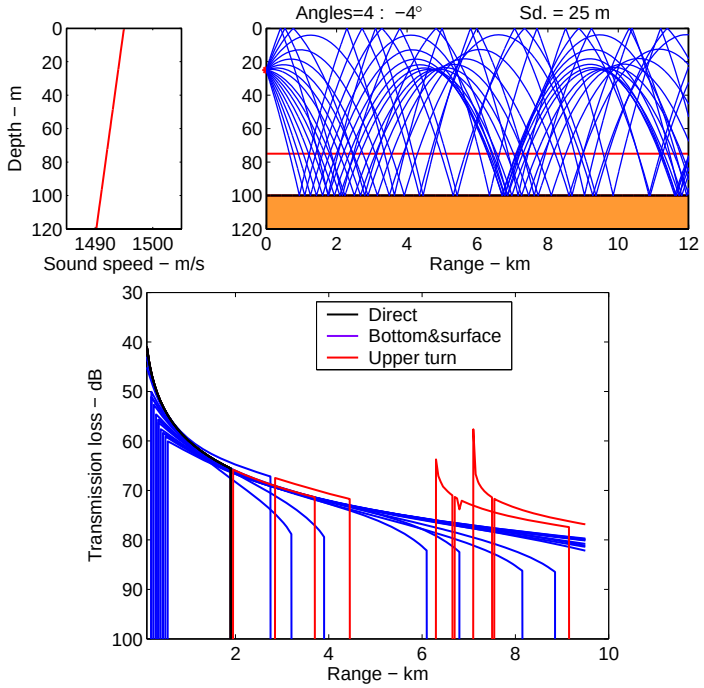

Figure 26. Transmission in a waveguide with water depth 100 m and up to the distance of 10 km, with source depth of 25 m and receiver depths of 75 m.
The upper part of the figure shows the sound speed profile (left) with constant negative gradient, c(z) =1495-0.04 z. The upper right part of the figure shows the trajectories of ten rays in the angle interval of ± 5 degrees. The lower part of the figure shows the calculated geometrical transmission loss as function of range.

The transmission loss curves are color-coded with information about the ray history as defined by the classes of Table 1. The black curve is the direct ray reaching out to a maximum distance of about 2 km. The blue curves are contributions of the rays that have been reflected both in the sea surface and the bottom one or more times. The red curves represent the contributions of the rays that have gone through a turning point before reaching the sea surface. Notice the effect of the caustics as seen from the low transmission loss at about 6.5 km and 7 km.

In figure 27 we compare the PlaneRay results OASES calculation of the transmission loss as function of range for the frequencies of 50, 100, 200 and 400 Hz. For this case the basis is the calculation of 2*400 rays in the interval ± 60° and with 12*4=48 interactions were included in the synthesis of the time and frequency responses.

The general agreement is quite good, but we notice some difference in the transmission losses for ranges slightly above 6 km, particularly noticeable for the frequency of 100 Hz and 200 Hz. This is probably caused by inaccurate calculations of the contributions of the refracted arrivals at these ranges, as can be seen from Figure 26. Some of discrepancies between the PlaneRay and the OASES results may be caused by different sampling densities of the sound speed profile. In the PlaneRay calculation a depth sampling interval of 0.5 m was used, but the OASES calculation used a staircase approximation with step size of 10 m. This difference in effective sound speed profile may cause differences in details of the sound field.

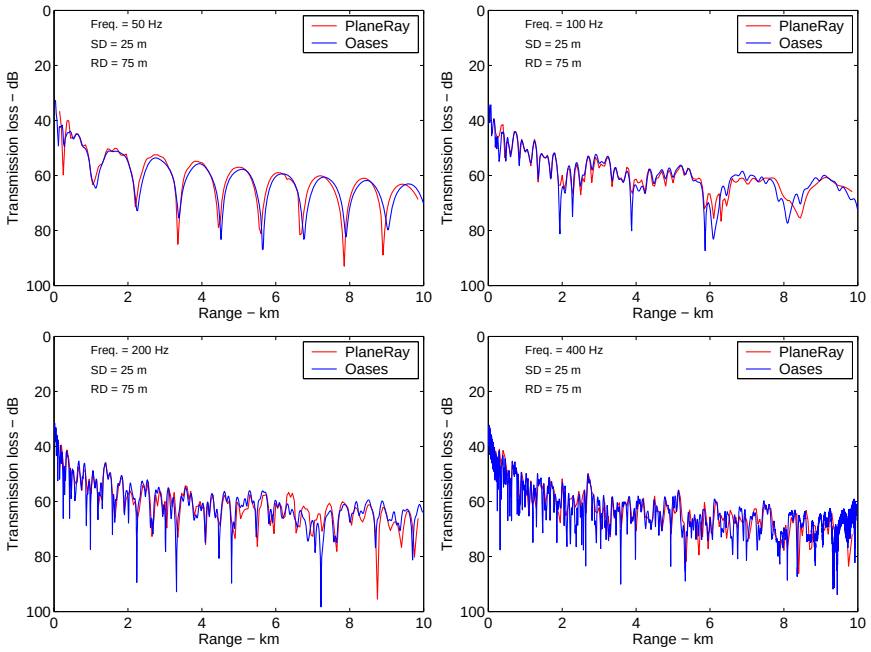

Figure 27. Transmission loss in dB as function of range for the frequencies 25 Hz, 50 Hz, 100 Hz and 200 Hz for the case of a negative gradient shown in Figure 26. The red curves are calculated by ray tracing and the PlaneRay model, the blue by the OASES model using the wave number integration technique.

Next, we consider the situation with the same geometry, but with a sound speed increasing linearly with depth, as

$$c(z) = 1495 + 0.04 \cdot z. \tag{26}$$

The profile and the some of the eigenrays to a receiver at 8 km are shown in Figure 28 and the transmission loss calculations are shown in Figure 29.

The transmission loss agrees generally with the OASES results, but the there are differences in the details. Some of these differences may be attributed to the different ways of sampling the sound speed profile as mentioned before.

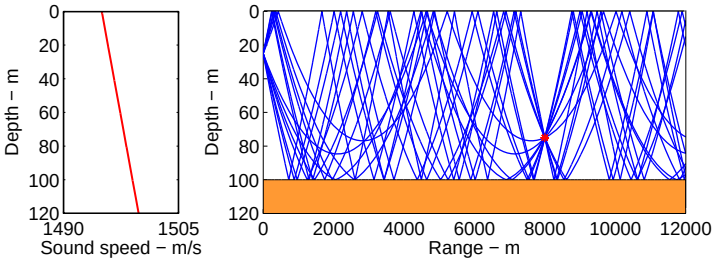

Figure 28. Eigenrays between a source at depth 25 m to a receiver at distance of 8000 m and depth 75 m. The sound speed is given as $c(z) = 1495 + 0.04 \cdot z$.

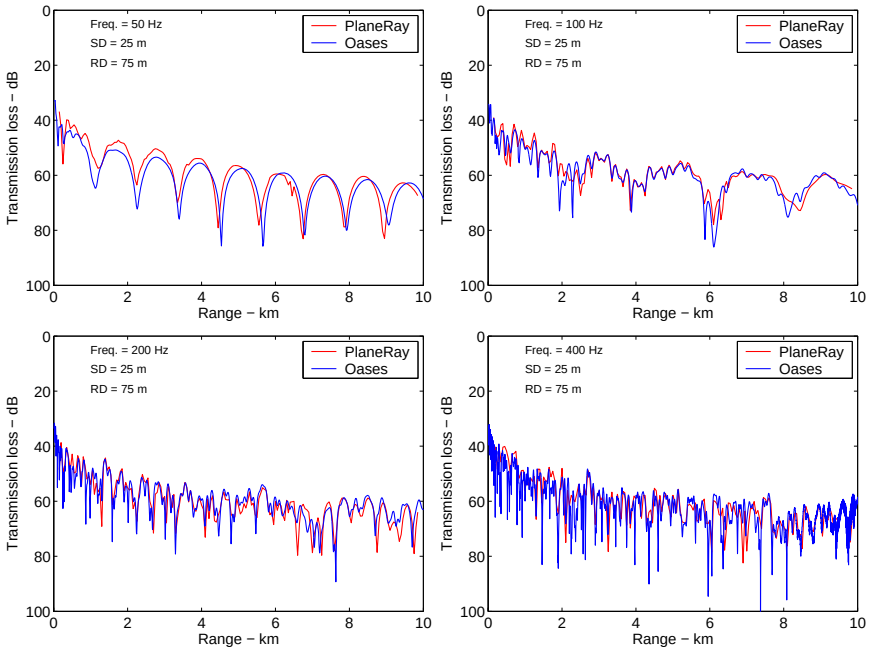

Figure 29. Transmission loss in dB as function of range for the selected frequencies 25 Hz, 50 Hz, 100 Hz and 200 Hz for the case of a positive gradient as shown in Figure 26. The red curves are calculated by ray tracing and the PlaneRay model, the blue by the OASES model using the wave number integration technique.

3.3 Propagation in a sound channel

We consider a case with a sound speed channel at 100 m depth in 500 m of water. Figure 30 shows the sound speed profile and a selection of rays spanning the interval of -30° to 30° and emitted from a source at 300 m depth. Figure 31 shows the eigenrays connecting the source at 300 meter with a receiver at 100 m depth and distance 8500 meter from the source.

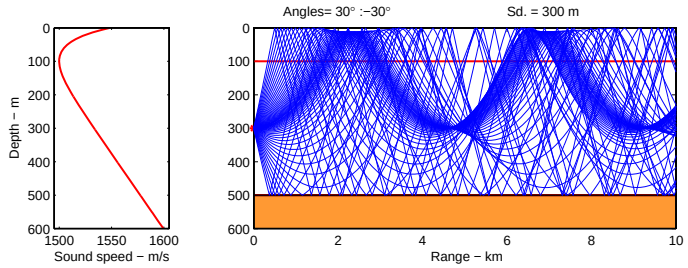

Figure 30. Propagation in a sound channel. Left sound speed profile. Right: Traces of a selection of rays spanning the angles of -30° to 30° emitted at a source depth of 300.

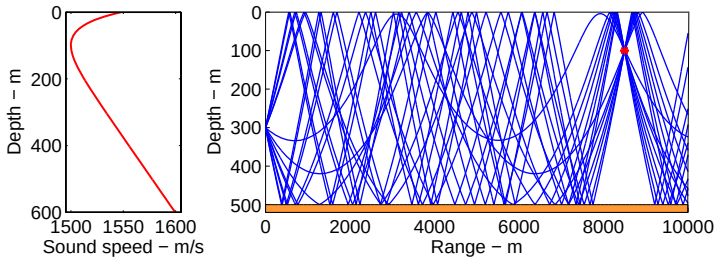

Figure 31. Propagation in a sound channel. Left sound speed profile. Right: eigenrays connection a source at a depth of 300 m with a receiver at 100 m depth and distance 8500 m from the source.

Figure 32 shows the geometrical part for the transmission loss as function of range. The various contributions are identified as indicated in the legend. For instance, the red contributions that are dominant at the two range intervals 3 to 4 km and 8 to 9 km are from rays that have been through both upper and lower turning points and consequently not been reflected from either the surface or the bottom. The green contributions from 2 to 4 km and from 8-9 km are from rays that have been reflected from the sea surface and gone trough lower turning points before striking the bottom.

Figure 33 shows the time plots for the several different ranges up to 10 km. The various contributions are colour coded in the same way as in Figure 32. We notice in particular the contribution in green and red as coming from rays the have not interacted with the bottom as indicated above. The blue contributions in the representations of both Figures 32 and 33 are rays reflected both in the sea surface and in the bottom one or more times.

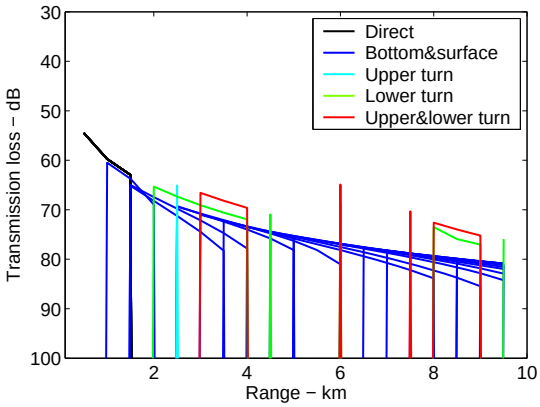

Figure 32. Transmission loss as function of range for a source depth of 300 m and receiver depth 100. The contributions from the various ray paths are colour as indicated in the legend.

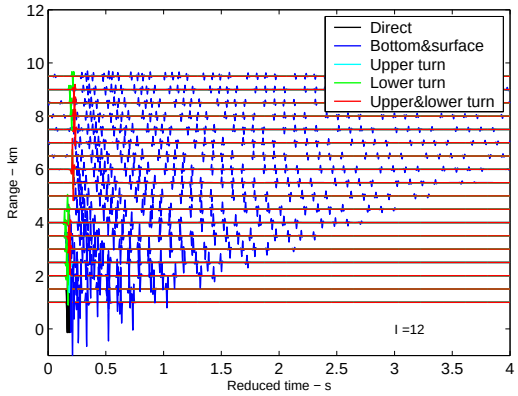

Figure 33. Time response at various distances for transmission of a Ricker pulse from a source at 300 m to a receiver at 100 m. The contributions of the various ray paths are colour coded as indicated in the legend.

Because of the upward refraction sound speed profile a great number of rays will strike the bottom at angles lower the critical angle and therefore the length of channel impulse response may be very long as can bee seen from Figure 31. In Figure 32 and 33 the number of bottom interactions included in the calculations is arbitrarily limited to 12 interactions.

3.4 Range dependent cases

3.4.1 The ARL wedge

The paper by Stotts et al. (2003) reported using a ray trace model and plane wave reflection coefficients to model propagation loss in a wedge. Their results showed excellent agreement with other propagation models for a selected frequency of 80 Hz. Although the principle of using ray theory is the same as used in PlaneRay, the implementations are very different particularly the algorithm for finding the eigenrays and therefore it was found interesting to test PlaneRay on the same case.

The wedge has a down slope angle of 3 degrees starting with water depth 100 m at the source location as shown in Figure 34 (left). The source depth is 47 m and the receivers are at 30 m depths. The bottom is modelled with a 200 m thick sediment layer modelled as a fluid with sound speed 1784 m/s, density 1970 kg/m^3, and attenuation 0.547 dB/(m kHz). Below this layer the is a half space with compressional speed 5790 m/s, density 9800 kg/m^3 and zero sound speed. This shear speed value is quite unrealistic but for frequency considered the effect of the deeper half space is of negligible importance. Figure 34 (left) shows the situation and some of the eigenrays connecting the source to a receiver at range 2000. Figure 34 (right) shows that the transmission loss obtained by the PlaneRay model is in excellent agreement with the result of the ARL coupled mode program for the frequency of 80 Hz. Figure 35 shows the time response as function of range (left), and the transmission loss as function of rage and frequency obtained by the ray tracing.

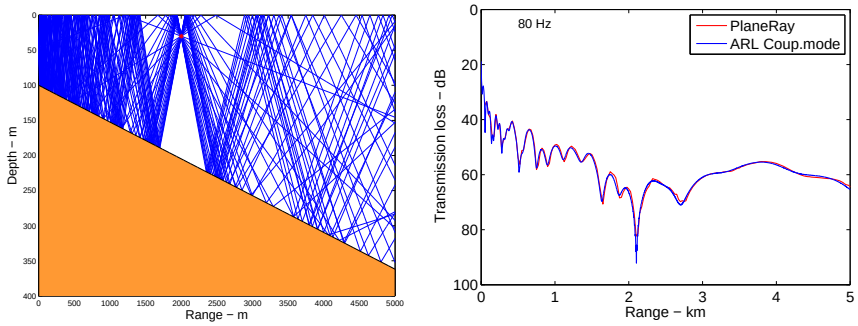

Figure 34. Example of eigenrays, in this case to a receiver at range 2000 meter and depth 30 meter(left) and transmission loss as function of range for a frequency of 80 Hz.(right) The PlaneRay result (red curve) is compared with the result of ARL coupled mode code calculation (blue)

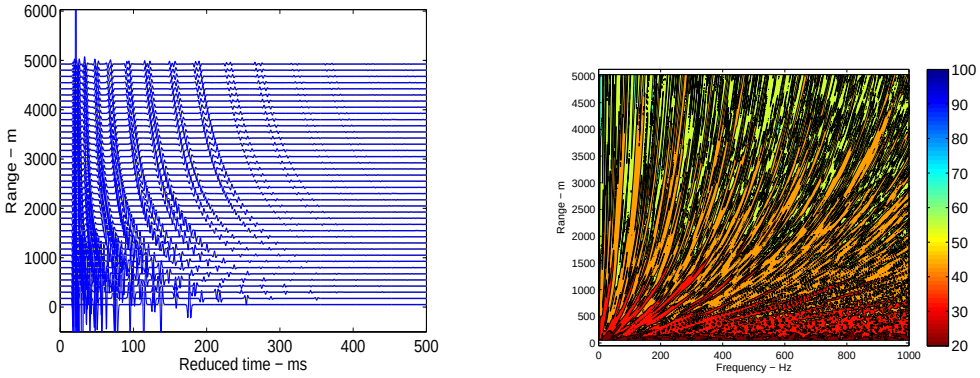

Figure 35. Time response for a number of receivers with ranges out to 7500 m (left) and transmission loss (dB) as function of range and frequency (right).

3.4.2 Down slope propagation with positive sound speed gradient

Figure 36 shows an example of down slope propagation with a positive sound speed gradient. The accuracy in finding the eigenrays is quite good as can be seen. Figure 37 shows some results of the calculated transmission losses, this time with the result from the RAM model using the parabolic approximation. At the lowest frequency of 25 Hz the agreement is not very good because of the low frequency limit for the validity of the ray tracing approximation, as commented on earlier. The higher frequencies results agree in the main features, but not in details. This is probably due to the difference in sampling density of the sound speed profile as discussed earlier, 0.5 m for the PlaneRay calculations and 5 m for the RAM.

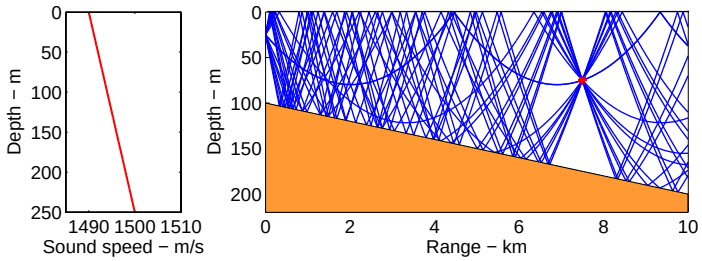

Figure 36. Eigenrays between a source at depth 25 m to a receiver at distance of 7500 m and depth 75 m over a bottom with constant slope from 100 to 200 meters over 10 km. The sound speed is given as $c(z) = 1495 + 0.04 \cdot z$.

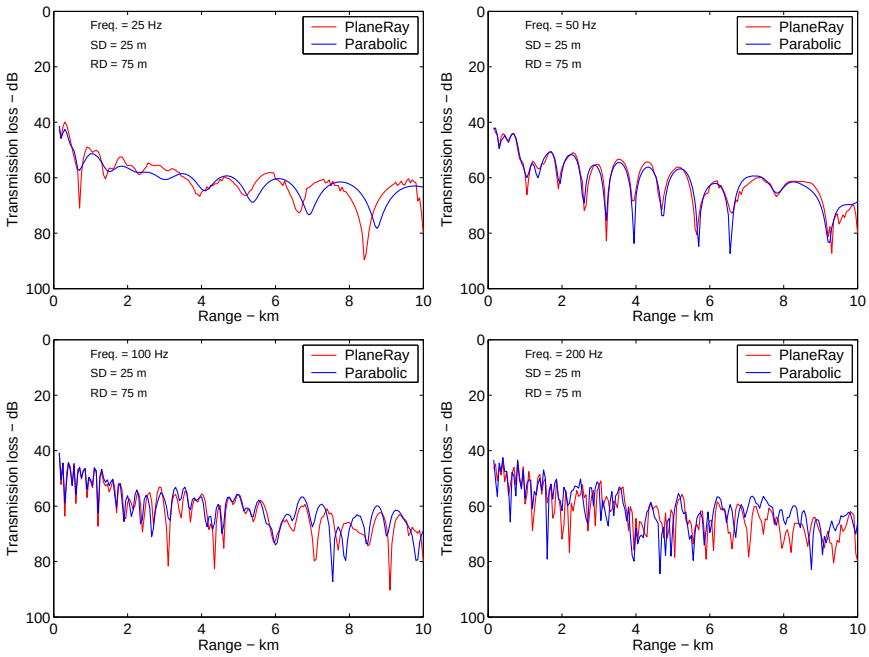

Figure 37. Transmission loss in dB as function of range for the selected frequencies 25 Hz, 50 Hz, 100 Hz and 200 Hz for down slope propagation with positive sound speed gradient shown in Figure 36. The red curves are calculated by ray tracing and the PlaneRay model and the blue curve by the RAM model using the parabolic approximation.

3.4.3 Range dependent bottom parameters

In this section we investigate the PlaneRay code for modelling situations where the bottom parameters may vary with range .We therefore consider the otherwise simple case with constant water depth and constant sound speed profile. The situation under investigation is depicted in Figure 38. The water depth is everywhere 300 m. The bottom, for the most part, consist of a fluid-like sediment layer over a homogeneous solid half space, but in a finite range interval there is a salt dome coming from a very large depth and up to the sedimentary layer. The assumed physical parameters for the sediment, rock and salt are given in Table 3. The location of the salt dome and the thickness of the sediment layer are free parameters that are varied with values given in Table. The source depth is in all case 25 m and the receiver depth is 75 m.

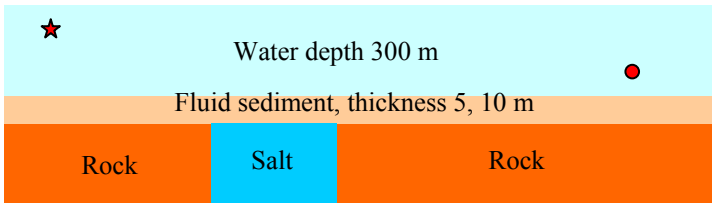

Figure 38. Water over a two layer bottom with a salt dome intrusion

Table 3. Physical parameters

	Water	Sediment	Rock	Salt
Sound speed m/s	1500	1800	2400	5300
Sound attenuation - dB/wavelength	0	0.5	0.5	0.5
Density kg/m^3	1000	1800	2000	2000-2500
Shear speed - m/s	0	0	1000	2000-2200
Shear attenuation – dB/wavelength	0	0	0.5	0.5

Figure 39 shows examples of the bottom reflection loss for two cases (1) sediment layer over rock and (2) sediment layer over salt; both cases with sediment layer thickness of 5 m. For the case with sediment layer over rock (left in Figure 36), there is a significant reflection loss at very low frequencies between 20° and 40° and this loss is caused by shear wave conversion in the rock which has a shear speed of 1000 m/s.

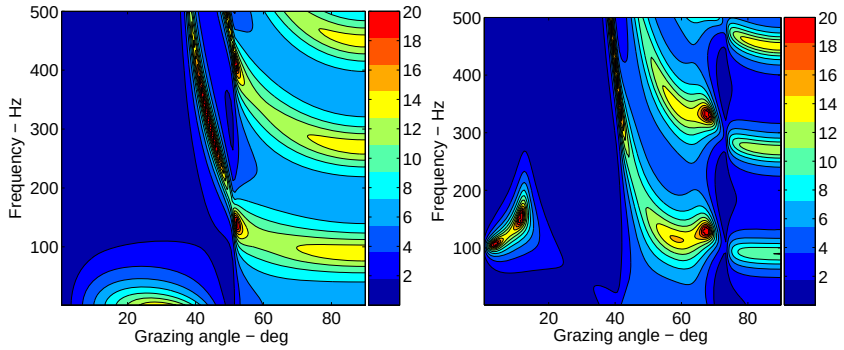

Figure 39. Bottom reflection loss (dB) as function of frequency and incident angle for: 5 m sediment layer over rock (left), and 5 m sediment layer over salt (right).

In the case with sediment layer over salt there are significant reflection losses in the frequency range of 100 to 200 Hz and at angles between 0° and 20°. This loss is caused by conversion to interface wave propagating along the sediment-salt interface. The existence of this anomalous loss is, however, very dependent on small variations of the geoacoustic parameters of the layer and half space, and may disappear completely for other selection of parameters.

We now consider the case where the bottom is composed of a 5 m fluid-like sediment layer over an infinite elastic half space with the parameters of salt as given in Table 1. This may not be a realistic, but it is a useful for the testing and validation of the modelling.

Figure 40 shows the time responses as function of reduced travel time and range. The red lines are the result of plotting Equation (24) for the angles of 5°, 10°, and 20°. Notice the changes in amplitudes for arrivals later than the 5° line and another reduction at about 10°. These changes or reductions in amplitudes are a direct consequence of the anomalous reflection loss shown in Figure 35 (right).

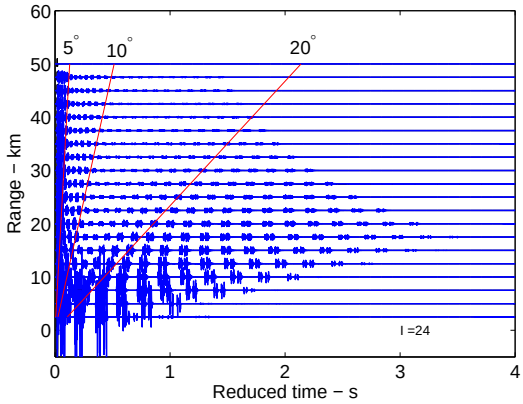

Figure 40. Time response in reduced time for receivers at distance up to 50 km. when the bottom has a 5 m sediment layer with sound speed 1800 m/s, density 1800 kg/m^3, over an elastic half space with compressional sound speed of 5300 m/s, shear speed 2000 m/s, density of 2500 kg/m^3. All absorptions are 0.5 dB/λ.

Figure 41 compares the transmission losses calculated by PlaneRay and OASES using the same parameters as used to calculate Figure 40. The two set of transmission loss agree quite well with exceptions of some points at the extreme distance of 50 km.

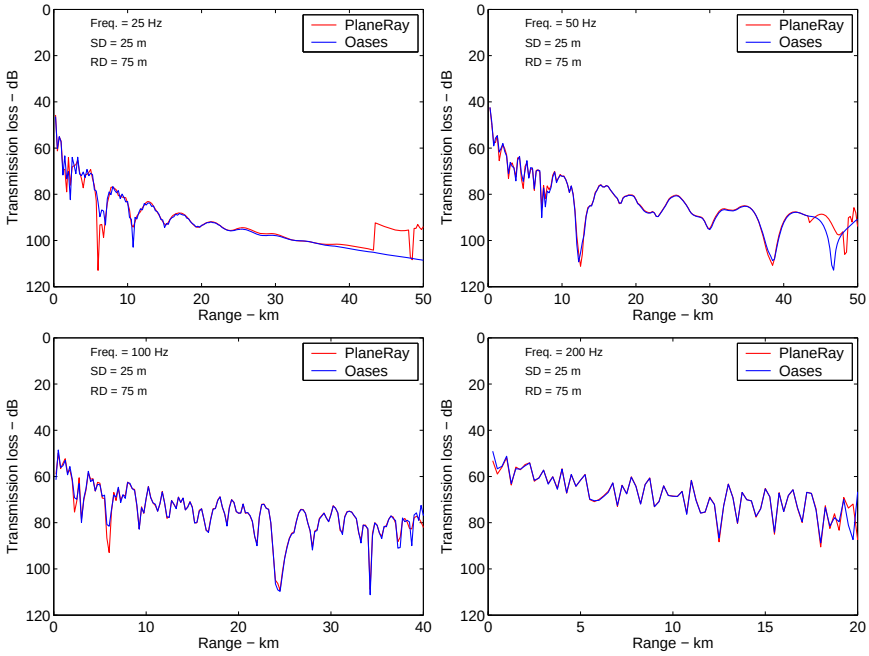

Figure 41. Transmission loss versus range. The bottom is a 5 m fluid sediment layer over an infinite half space of rock with sound speed 2400 m/s, shear speed 1000 m/s, density 2000 kg/m^3 and absorption 0.5 dB per wavelength. The results of PlaneRay are compared with OASES for the frequencies of 25 Hz, 50 Hz, 100 Hz, and 200 Hz.

The next example models the effect of a 5 km wide salt dome covered by a 5 m sediment layer and located between 15 km and 20 km from the source position, see Figure 38. Figure 42 shows the time responses as function of range and the transmission loss as function of range and frequency.

Figure 43 compares transmission loses with the presence of a salt dome (labelled “Salt dome”) with the situation without a salt dome (labelled “Rock only”), both cases calculated by the PlaneRay. Up to a distance of 15 km the two sets of results are identical as expected. At longer ranges the transmission losses are different, but not very significantly which indicates the presence of a salt dome of this size has relative little importance.

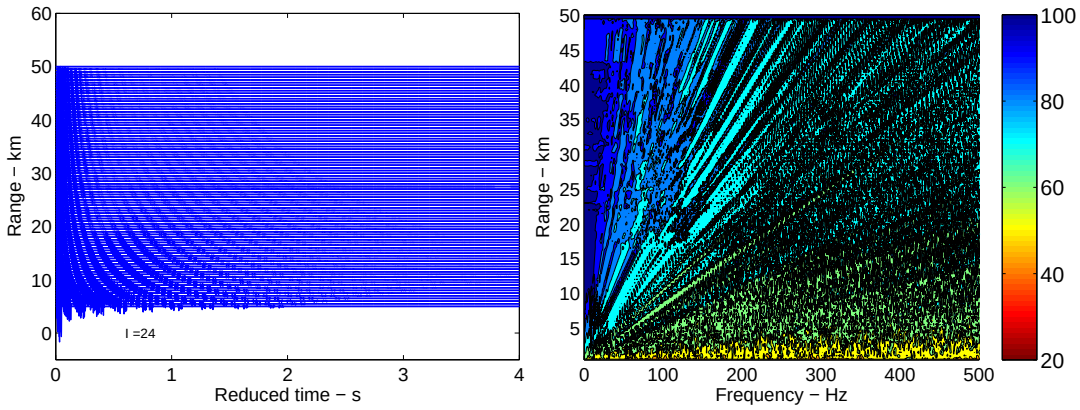

Figure 42. Modelling the effect of a 5 km salt dome located between 15 km and 20 km, thickness of sediment layer is 5 m. Left: Time responses (left) and transmission loss in dB (right).

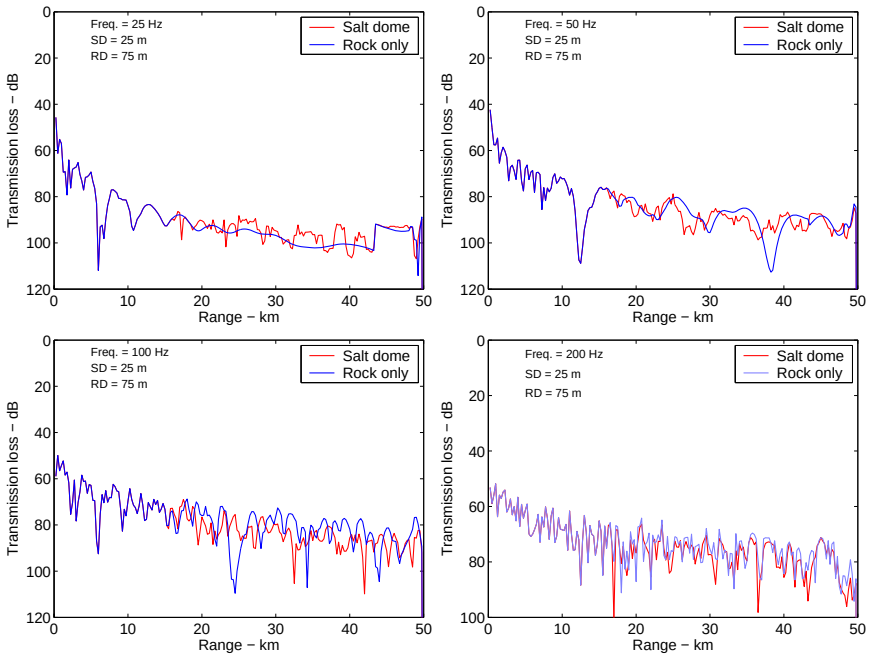

Figure 43. Transmission loss versus range for the frequencies 25 Hz, 50 Hz, 100 Hz and 200 Hz Layered bottom with a 5 m thick fluid sediment over rock in the range with a salt dome in the interval from 15 to 20 km. The parameters are given in Table 3.

In the next example we consider a wider salt dome 10 km wide, located at the range between 15 km and 25 km. The time plots in Figure 44 show that the presence of the salt dome increases the

bottom reflection loss, and therefore the transmission loss, for rays with angles steeper than approximately 10° for longer ranges than 15 km.

Figure 45 shows the transmission loss as function of range for selected frequencies and demonstrate that the increase in transmission loss is frequency dependent. For instance, we observe significantly increased transmission loss for 50 Hz for longer ranges than 20 km. For 25 Hz and 100 Hz there are only small changes and at 200 Hz there no change in the transmission. All this agree with, and is as expected, from the frequency dependence of the bottom reflection loss which was displayed in Figure 39 (right). This figure shows anomalous high reflection loss for very low grazing angels at 100 Hz, which converts to 50 Hz in the case of a 10 meter layer.

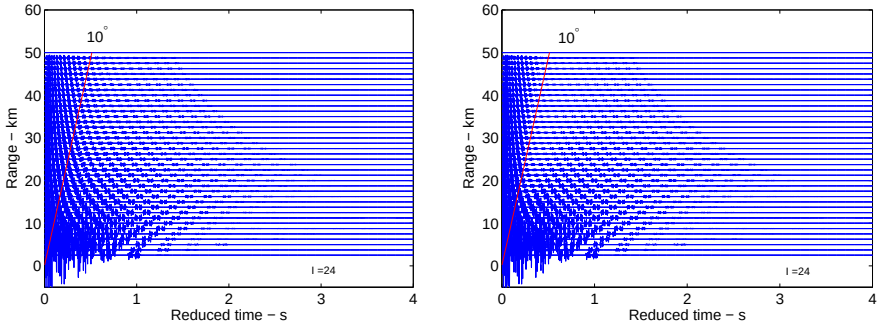

Figure 44. Time responses as a function of range. Left: 10 m thick sediment layer over rock over the whole range. Right: Salt dome located between 15 km and 25 km.

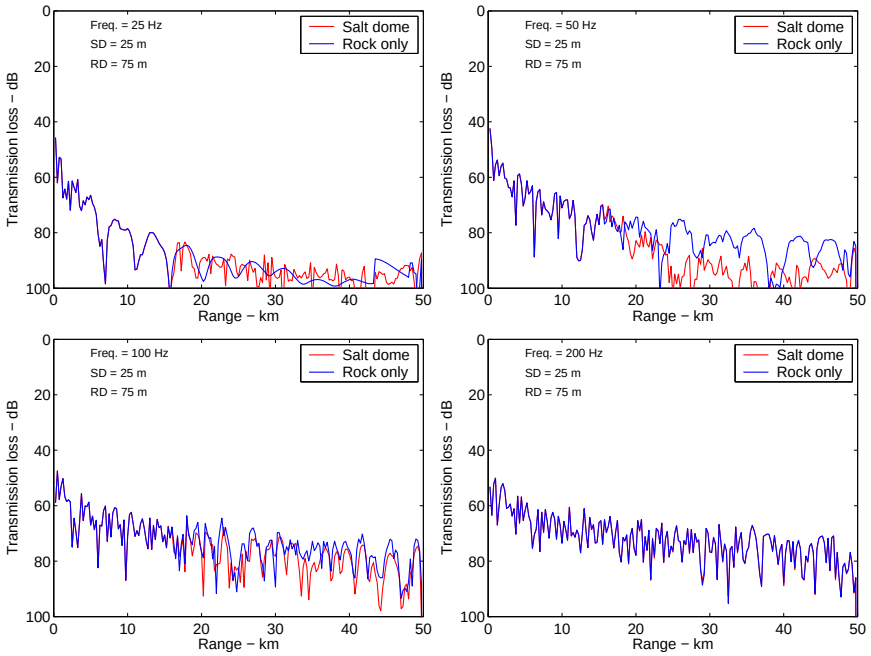

Figure 45. Transmission loss versus range for the frequencies 25, 50, 100 and 200 Hz Layered bottom with a 10 m thick fluid sediment over rock in the range with a salt dome in the interval from 15 to 25 km. The parameters are given in Table 3.

4 Dispersion analysis

We end this report with a comment on the relationship between ray theory and normal mode theory. Figure 46 shows PlaneRay simulated time signal at a receiver at 75 meter depth and a distance of 10 km from a source at 25 meter. The water depth is 100 meter and the sound speed is constant, 1500 m/s, the sound speed of the homogeneous bottom is 1700 m/s.

The lower part shows the result of a time - frequency analysis, also called a Gabor analysis. This is accomplished by performing Fourier analysis of sliding-window selections of the time signal to determine the frequency components of the signal as function of time. When the distance between the source and receiver is known, time can be converted to speed, in this case to group speed. The lower part of Figure 46 shows the group speed of the received signal as function of frequency. There are a number of modes, two strong modes at 50 Hz and three or four modes at 100 Hz.

In this simple case constant water depth D, and with sound speeds c_0 and $c_1$and densities ρ_0 and ρ_1 respectively for the water and the bottom the dispersion equation giving the phase speed v_m for the mode number m is given as:

$$\tan\left[\left(m-\frac{1}{2}\right)\pi+\frac{\omega D}{v_m}\sqrt{\left(\frac{v_m}{c_0}\right)^2-1}\right]=\frac{\rho_0\sqrt{1-\left(\frac{v_m}{c_1}\right)^2}}{\rho_1\sqrt{\left(\frac{v_m}{c_0}\right)^2-1}} \quad . \tag{27}$$

This equation can easily be solved numerically after which the group speed w_m of mode number m is obtained by calculating.

$$w_m=\frac{v_m}{1-\frac{\omega}{v_m}\frac{\partial v}{\partial \omega}} \tag{28}$$

Figure 47 shows the theoretical results for group speed versus frequency obtained directly from the relevant dispersion equations, Equations (27) and (28), and we see that the close resemblance with the result of the dispersion analysis. This is a demonstration of the connection between mode theory and ray theory which is added here only for tutorial reasons.

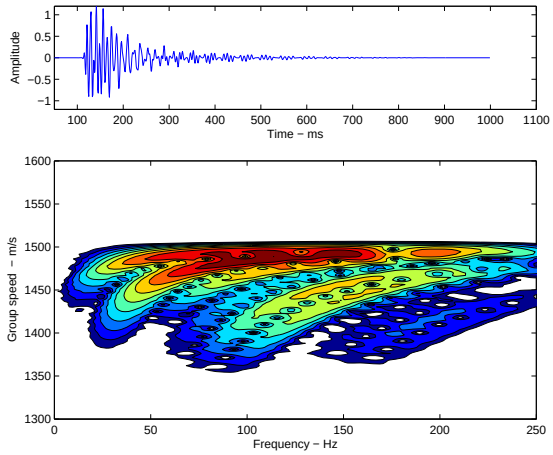

Figure 46. Dispersion analysis of the received signal in an acoustic wave guide: Upper: Received time signal at a distance of 10 km from the source. Lower: Result of the time-frequency analysis showing the group speed as function of frequency.

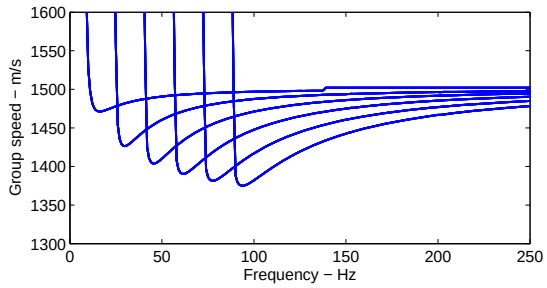

Figure 47. Group speed as function of frequency for the first 6 modes of a Pekeris' wave guide with water depth 100 m and sound speed of 1500 m/s. The sound speed in the bottom is 1500 m/s and the density is 1500 kg/m^3.

5 Conclusions

The PlaneRay model is an acoustic propagation model intended for use in range dependent environments, particularly in situations where the structure and material properties of the bottom vary with range. An essential feature of the model is the unique sorting and interpolation scheme for efficient determination of large number of eigenrays. The complete acoustic field at a given receiver location is calculated by coherent addition of the contributions of a large number of eigenrays. No rays are traced into the bottom, but the bottom interaction is modeled by local plane wave reflection coefficients. The bottom can be a fluid-like sedimentary layer over an elastic half space and the layer thickness, the sound speeds and the densities can vary with range. The sound speed of the water may vary with depth, but not with range.

Ray tracing calculation is, by definition, frequency independent and therefore the calculations of ray trajectories through the water column are not dependent on frequency. Frequency dependency is introduced afterwards with the introduction of the bottom or surface reflection coefficient in the bottom, by layering and absorption, or by diffuse scattering of rough ocean surface or bottom

interface. Therefore the ray tracing and the determination of the eigenrays need to be done only once for each scenario, i.e. for a fixed bottom topography, sound speed profile and source and receiver depths. Since these calculations are the most computational intensive parts of the code, the PlaneRay model is quite efficient for broad frequency band calculations and consequently for the calculation of time responses by Fourier transformation of the frequency transfer functions.

During the development of the code we have found that time responses are very useful for the interpretation and understanding of the features of a sound field.

There are two main limitations to the overall accuracy and validity of the calculations. Since ray tracing technique is fundamentally a high frequency approximation of the solution of the wave equation, there are basic limitations with low frequency propagation modelling, for instance limited to 50 Hz in 100 m of water depths and 20 Hz in 300 m water. The validity and accuracy of using plane ray reflection coefficient to represent the effects of a layered bottom can also be bottom questioned. At present this is not fully investigate or understood, but one condition is clearly related to the heights of the source and receiver above the water bottom interface and the thickness of the layer related to the wavelength of the frequency.

The second main limitation is due to the numerical accuracy of the determination of the eigenrays, most serious in the calculation of the ray amplitude or the transmission loss. These inaccuracies are of more practical nature and can be reduced by refinements in the calculations at later stages.

This report has described the main features of the Plane Ray model and presented the results of a number of test cases with comparison with the results for other more established models. Additional examples and comparisons are found in Smedsrud and Tollefsen (2007).These examples should give a good impression of what the model can do and its limitations. However, this is not a manual for using the code, which eventually will be prepared later.

The main conclusion is that ray tracing modelling may be quite useful technique for applications moderately range dependent environments and, as such be a valuable addition and alternative to other models with different advantages and limitations.

References

Ainslie A. M., Conditions for the excitation of interface waves in a thin unconsolidated sediment layer, J. Sound and Vibration, 268, 249-267 (2003).

Chapman, N.R., S. Chin–Bing, D. King and R.B. Evans, Benchmarking geoacoustic inversion methods for range-dependent waveguides, IEEE J. Oceanic Eng., 28, 320-330, (2003).

Clay C. S. and H. Medwin, *Acoustical Oceanography: Principles and Applications*, Wiley-Interscience, USA, (1977).

Collins M. D., A split-step Pade solution for parabolic equation method, J. Acoust. Soc. Am. **93**, 1726-1742 (1993).

Collins M. D., User guide for RAM version 1.0 and 1.0p, (ftp:// ram.nrl.navy.mil/pub/ RAM/), (2001).

Gerstoft P., SAGA User Manual 4.1: An inversion software package, SM-333, SACLANT Undersea Research Centre, La Spezia, Italy (1997).

Hovem J. M. and Å. Kristensen, Reflection loss at a bottom with a fluid sediment layer over a hard solid half-space, J. Acoust. Soc. Am. **92**(1), 335-340 (1992)

Hovem J. M., Marine Acoustics: *The Physics of Sound in Underwater Environments*, (To be published by Peninsula Publishing, Los Altos, CA, and Applied Research Laboratories, The University of Texas at Austin, Texas), 2008.

Jensen F. B. and M. C. Ferla, "SNAP: The SACLANTEN normal-mode acoustic propagation model," SM-121, SACLANT Undersea Research Centre, La Spezia, Italy (1979).

Jensen F. B., W. A. Kuperman, M. B. Porter, and H. Schmidt, *Computational Acoustics*, AIP Press, New York Jersey, (1993).

Officer, C. B. *Introduction to the theory of sound transmission*. McGraw-Hill, New York City, 1958.

Pekeris A. L., The theory of propagation of explosive sound in shallow water, Geol. Soc. Am. Mem. **27** (1948).

Schmidt H., OASES 1.6: Application and upgrade notes, Massachusetts Institute of Technology, Cambridge, MA (1993).

Schmidt H., SAFARI: Seismo-acoustic fast field algorithm for range independent environments. User's guide, SR-113, SACLANT Undersea Research Centre, La Spezia, Italy (1987).

Smedsrud, M., and Tollefsen, D. "Test of the PlaneRay propagation model for selected low-frequency scenarios" FFI report 2007/00921, Norwegian Defence Research Establishment, Kjeller, Norway, 2007

Stotts, S. A., D. P. Knobles, R. A. Koch, D. E. Grant, K. C. Foche, and A. J. Cook "Geoacoustic inversion in range-dependent environments using a plane wave reflection coefficient approach." J. Acoust. Soc. Am.**115** (3),1078-1102, March 2004.

Tindle C. T. and G. E. J. Bold, Improved ray calculations in shallow water, J. Acoust. Soc. Am. **70**(3), 813-819 (1981).

Tollefsen, Dag " Thin-sediment shear induced effects on low frequency broadband propagation in a shallow continental sea", J. Acoust. Soc. **104**(5), 2718-2726, 1998.

Westwood, E. K and C. T. Tindle, Shallow water time simulation using ray theory, J. Acoust. Soc. Am. **81**, 1752 -1761 (1987).
Westwood, E. K and P. J. Vidmar, Eigenray finding and time series simulation in a layered-bottom ocean, J. Acoust. Soc. Am. **81**, 912 -924 (1987).